CORE COSMOLOGY LIBRARY: PRECISION COSMOLOGICAL PREDICTIONS FOR LSST

Husni Almoubayyed,[1] David Alonso,[2,3] Jonathan Blazek,[4,5] Philip Bull,[6,7] Jean-Éric Campagne,[8]
N. Elisa Chisari,[3] Alex Drlica-Wagner,[9] Zilong Du,[10] Tim Eifler,[11,12] John Ellison,[10] Renée Hlozek,[13]
Mustapha Ishak,[14] Shahab Joudaki,[3] Matthew Kirby,[15] David Kirkby,[16] Elisabeth Krause,[17]
C. Danielle Leonard,[1] Christiane S. Lorenz,[3] Phil Marshall,[18] Thomas McClintock,[15] Sean McLaughlin,[19]
Alexander Mead,[20] Jérémy Neveu,[8] Stéphane Plaszczynski,[8] Javier Sanchez,[16] Sukhdeep Singh,[1,21]
Anže Slosar,[22] Antonio Villarreal,[23] Michal Vrastil,[24] and Joe Zuntz[25]

(LSST Dark Energy Science Collaboration)

[1]McWilliams Center for Cosmology, Department of Physics, Carnegie Mellon University, Pittsburgh, PA 15213, USA
[2]School of Physics and Astronomy, Cardiff University, The Parade, Cardiff, CF24 3AA, United Kingdom
[3]Department of Physics, University of Oxford, Denys Wilkinson Building, Keble Road, Oxford OX1 3RH, United Kingdom
[4]Center for Cosmology and Astroparticle Physics, Ohio State, Columbus, OH 43210, USA
[5]Laboratory of Astrophysics, École Polytechnique Fédérale de Lausanne (EPFL), Observatoire de Sauverny, 1290 Versoix, Switzerland
[6]Department of Astronomy, University of California Berkeley, Berkeley, CA 94720, USA
[7]Radio Astronomy Laboratory, University of California Berkeley, Berkeley, CA 94720, USA
[8]Laboratoire de l'Accélérateur Linéaire, Université Paris-Sud, CNRS/IN2P3, Université Paris-Saclay, Orsay, France
[9]Fermi National Accelerator Laboratory, P. O. Box 500, Batavia, IL 60510, USA
[10]Department of Physics and Astronomy, University of California, Riverside, CA 92521, USA
[11]Jet Propulsion Laboratory, California Institute of Technology, Pasadena, CA 91109, USA
[12]Department of Physics, California Institute of Technology, Pasadena, CA 91125, USA
[13]Dunlap Institute for Astronomy and Astrophysics & Department for Astronomy and Astrophysics, University of Toronto, ON M5S 3H4
[14]Department of Physics, The University of Texas at Dallas, Richardson, TX 75083, USA
[15]Department of Physics, Univeristy of Arizona, Tucson, AZ 85721, USA
[16]Department of Physics and Astronomy, University of California, Irvine, CA 92697, USA
[17]Kavli Institute for Particle Astrophysics and Cosmology, Stanford, CA 94305-4085, USA
[18]SLAC National Accelerator Laboratory, Menlo Park, CA 94025, USA
[19]Stanford University, Stanford, CA, 94305, USA
[20]Department of Physics and Astronomy, University of British Columbia, 6224 Agricultural Road, Vancouver, BC V6T 1Z1, Canada
[21]Berkeley Center for Cosmological Physics and Department of Physics, University of California, Berkeley, California
[22]Brookhaven National Laboratory, Physics Department, Upton, NY 11973, USA
[23]Department of Physics and Astronomy, University of Pittsburgh, Pittsburgh PA 15260
[24]Institute of Physics CAS, Prague, 182 21, CZ
[25]Institute for Astronomy, Royal Observatory Edinburgh, Edinburgh EH9 3HJ, UK

ABSTRACT

The Core Cosmology Library (CCL) provides routines to compute basic cosmological observables with validated numerical accuracy. In the current public version, predictions are provided for distances and background quantities, angular auto- and cross-spectra of cosmic shear, lensing of the microwave background and clustering, and the halo mass function. The output of these routines has been successfully compared, to a numerical accuracy level documented herein, against the results of independent implementations of the same predictions. Fiducial specifications for the expected galaxy distributions and clustering bias for the Large Synoptic Survey Telescope are also included, together with the capability of computing redshift distributions for a user-defined photometric redshift model. CCL is written in C, with a Python interface. JAB: General comment: Do we want to make more clear that we are always referring to numerical accuracy rather than accuracy with "reality?" Or is this obvious?

Contents

1. INTRODUCTION

Volunteer(s) in charge: Mustapha Ishak, Elisa Chisari
Section ready for revision

Starting in the next decade, large-scale galaxy surveys will drive a new era of high precision cosmology (LSST Dark Energy Science Collaboration 2012; Green et al. 2011; Laureijs et al. 2011). Their overarching goal is to answer the question of the origin of cosmic acceleration. In other words, to elucidate the nature of "dark energy", broadly understood as a family of potential models: from a cosmological constant to a dynamical field and modifications of gravity; see for example (Carroll 2001; Peebles & Ratra 2003; Padmanabhan 2003; Copeland et al. 2006; Ishak 2007; Weinberg et al. 2013) and references therein. JAB: mention dark matter?

High precision constraints on dark energy models will be achieved by probing at the same time the expansion and growth history of the Universe over a long redshift baseline. For this purpose, it will be crucial to combine measurements of multiple cosmological probes: weak and strong gravitational lensing, the clustering of galaxies, baryon acoustic oscillations, distances to supernovae, and the abundance, clustering and gravitational lensing of galaxy clusters. Current weak lensing surveys have started to take this approach already (Joudaki et al. 2018; van Uitert et al. 2018; DES Collaboration et al. 2017; Krause et al. 2017). From a theoretical perspective, there are two challenges faced by the next generation of galaxy surveys.

The first one is to ensure that all probes are modeled accurately, [including cosmological, astrophysical, and observational effects,] MI: do we mean to leave the 3 of them here? to avoid potential biases in the final cosmological results. In the context of weak gravitational lensing, for example, phenomena that can lead to biases include the impact of baryons on the distribution of matter and the intrinsic alignments of galaxies (e.g. van Daalen et al. 2011; Semboloni et al. 2011; Troxel & Ishak 2015; Krause et al. 2016; Blazek et al. 2017). In the context of galaxy clustering, effects such as magnification of number counts and redshift space distortions need to be included in the models (Alonso & Ferreira 2015; Ghosh et al. 2018).

Second, even standard cosmological quantities in the simplest models, such as distances in a ΛCDM cosmology, have to be predicted to a validated degree of accuracy. Achieving this objective is not always trivial, as computing these quantities generally requries, for example, numerical integration or interpolation, both of which are prone to numerical error. To guarantee the validity of our predictions, comparisons must be performed between different numerical tools to ensure no

deviations are present MI: to ensure the desired accuracy.

Faced with these challenges, the Dark Energy Science Collaboration (DESC), one of the science collaborations of the Large Synoptic Survey Telescope (LSST), has built a comprehensive software tool that satisfies the needs of the next generation of cosmological analysis. MI: I suggest some rewording to connect the sentence before to the next one. This paper presents the Core Cosmology Library[1] (CCL). CCL is a library for making predictions that are validated to a well-documented numerical accuracy for the purpose of constraining cosmology. While CCL was built with LSST in mind, our goal was to produce user-friendly, well-documented, adaptable software that can be used in any theoretical modeling work in cosmology.

CCL computes standard cosmological functions including the Hubble parameter, cosmological distances, density parameters, the halo mass function, halo bias and linear growth functions. It calculates the matter power spectrum using various methods including common approximations, by calling external software such as CLASS (Blas et al. 2011), or emulators such as the "Cosmic Emulator" of Lawrence et al. (2017). It computes 2-point angular power spectra and correlation functions from various probes, going beyond the Limber approximation.

CCL's overall structure is illustrated in Figure 1. Our implementation has support for spatially flat and curved Λ-Cold Dark Matter (ΛCDM) cosmologies, and wCDM cosmologies with the option of using a time-dependent equation of state. It also allows for cosmologies with multiple massive neutrino species and can be linked to external software for modified gravity predictions (hi_CLASS, Zumalacárregui et al. 2017) To do: Table 1 outdated.

This manuscript [paper?] is organized as follows. Section 2 describes the cosmological models and observables supported by CCL. In Section 3, we describe the details of the implementation of the quantities introduced in Section 2. Section 4 provides details of the validation tests performed and the accuracy achieved. Section 5 gives brief guidelines for usage of CCL, although we direct the reader to the software online repository, documentation and user manual for further information. We conclude in Section 6 with an outlook towards the integration of CCL in LSST pipelines and we outline future additions to the software.

---

[1] publicly available at https://github.com/LSSTDESC/CCL

2. COSMOLOGICAL MODELS AND OBSERVABLES

Volunteer(s) in charge: Renee **Section ready for revision**

The overarching goal of CCL is to allow seamless integration of different cosmological models of interest to LSST.

The cosmological components include the matter density parameter Ω_m, the dark energy density Ω_Λ, the radiation density Ω_g , the curvature density Ω_K, the neutrino density of both massless and massive neutrinos, given by $\Omega_{\nu,\mathrm{rel}}$ and $\Omega_{\nu,\mathrm{m}}$ respectively, and parameters for the equation of state of dark energy defined below. The normalization of the density fluctuations is established either in terms of the amplitude of the primordial power spectrum, A_s, which is a power-law of index n_s, or in terms of the RMS variance in spheres of $8\,h/\mathrm{Mpc}$ today, σ_8.

Currently, the following families of models are supported:

- Flat ΛCDM cosmology with parameters Ω_b, n_s, A_s or σ_8, Ω_m, Ω_Λ, and a cosmological constant dark energy model with equation-of-state $w = -1$.

- wCDM and the Chevallier-Polarski-Linder (CPL) model for dark energy and its redshift dependence, which adopts the following parametrization for w as a function of the scale factor, a (Chevallier & Polarski 2001 and Linder 2003),

$$w(a) = w_0 + w_a(1 - a). \tag{1}$$

- A universe with non-zero curvature (K) so that the curvature energy density parameter is the difference of the sum of the energy densities of the other components with respect to unity (flatness), i.e. $\Omega_K = 1 - \sum_i \Omega_i$.

- All of the above, plus an arbitrary, user-defined modified growth function (see description in Section 2.2).

- Relativistic neutrinos in combination with any of the above, specified by N_{eff} (the number of relativistic neutrino species in the early Universe) and by the number of massive neutrinos today (see next item).

- Massive neutrino species in combination with any of the above except the user-defined modified growth function, specified by either Σm_ν (which maps on to the density $\Omega_{\nu,\mathrm{m}}$ above), or by the individual masses of each of three neutrino species.
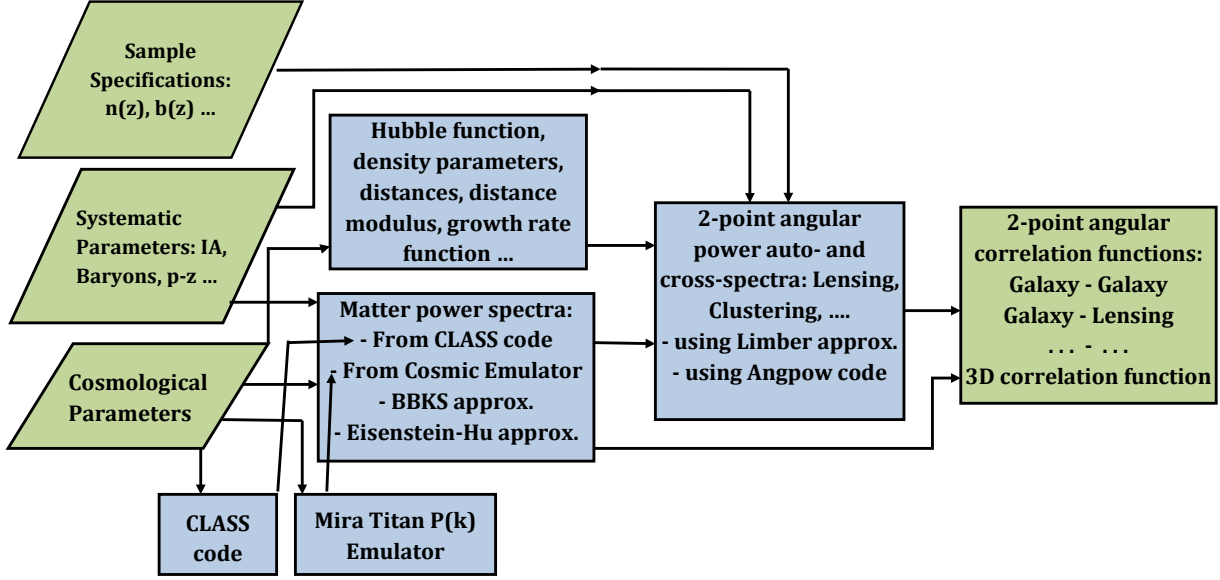
Figure 1. CCL structure flowchart. CCL is written in C with a Python interface. CCL routines calculate basic cosmological functions such as the Hubble function, density parameters, distances and growth function. It uses various methods to compute the matter-power spectrum including CLASS, "Cosmic Emulator" developed by Lawrence et al. (2017), or common approximations. It computes 2-point angular power spectra and correlation functions from various probes. CCL is designed to accommodate multiple methods to calculate cosmological observables. MI: Check if more needs to be done for the 3D correlation.

In the particular case of cosmologies with massive neutrinos, CCL allows the user to specify either a sum of masses, Σm_ν, or the individual mass of each of three neutrino species. In the former case, CCL will by default split Σm_ν into three neutrino masses which are consistent with the normal hierarchy (see, e.g. Lattanzi & Gerbino (2017) for a review). However, the user can alternatively ask for Σm_ν to be split either into masses consistent with the inverted hierarchy, or into equal masses. Each neutrino species is then checked for whether it is non-relativistic (massive) at $z = 0$, and this information is used in combination with the user-provided value of $N_{\rm eff}$ (the effective number of relativistic neutrino species in the early universe) to set the number of relativistic neutrino species.

Not all features of CCL are available for all models. For a guide to which predictions are available for each model, see Table 1. Note that if users install their own version of CLASS, CCL can then make predictions for a more extended set of cosmologies. Users should take care to understand the validity of the CCL assumptions for their own models.

2.1. Background cosmology

Volunteer(s) in charge: Renee,Shahab

The models that are specified above map directly onto cosmological observables such as the expansion rate of the Universe, which is parameterized through the Hubble parameter as

$$
\frac{H(a)}{H_0} = a^{-3/2}\Big(\Omega_m + \Omega_\Lambda a^{-3(w_0+w_a)} \exp[3w_a(a-1)]+
$$

$$
\Omega_K a + (\Omega_g + \Omega_{\nu,\rm rel})a^{-1} + \Omega_{\nu,\rm m}(a)a^3 \Big)^{\frac{1}{2}}, \qquad (2)
$$

MI: should we use Ω_{de} above in view of the general scale factor dependence used. which is a function of the energy density in the different components today and the scale factor. In this expression, we have assumed the CPL parameterization described above for the dark energy equation of state. $\Omega_{\nu,\rm m}(a)$ is the fractional energy density of massive neutrinos, calculated via

$$
\Omega_{\nu,\rm m}(a) = \frac{7}{8}\sum_{i=1}^{N_\nu}\frac{4\sigma_B}{c^3\rho_{\rm crit,0}}\left(\frac{T_\nu^{\rm eff}}{a}\right)^4 \left(\int_0^\infty dx\, x^2 \frac{\sqrt{x^2+(\mu^i)^2}}{\exp(x)+1}\right).
$$

$$(3)$$

Here, c is the speed of massless particles, $\rho_{\rm crit,0}$ is the critical density at $z = 0$, and $T_\nu^{\rm eff}$ is the present effective temperature of the massive neutrinos. $T_\nu^{\rm eff}$ is related to the temperature of the CMB via $T_\nu^{\rm eff} = T_{\rm CMB}T_{\rm NCDM}$, where $T_{\rm NCDM}$ is a dimensionless factor ($\simeq 1$) used by e.g. CLASS to set the ratio $\sum m_\nu/\Omega_{\nu,\rm m}$ to its experimentally measured value. Note that $T_{\rm NCDM}$ is used to modulate the effective temperature of massive neutrinos only; the temperature of relativistic neutrinos follows the usual relation. Finally, μ^i is a per-species mass-dependent dimensionless constant, given by $\mu^i = m_\nu^i c^2 a/(k_B T_\nu^{\rm eff})$.

Table 1. Cosmologies implemented in CCL.

Observable/Model	flat ΛCDM	ΛCDM+K	ΛCDM + m_ν	wCDM	$w_0 + w_a$	MG
Distances	✓	✓	✓	✓	✓	X
Growth	✓	✓	X	✓	✓	✓
$P_m(k,z)$	✓	✓	✓	✓	✓	X
Halo Mass Function	✓	✓	X	✓	✓	X
C_l, number counts	✓	X	X	✓	✓	X
C_l, weak/CMB lensing	✓	X	✓	✓	✓	X
Correlation function	✓	X	✓	✓	✓	X

The density parameters $\Omega_X(a)$ of a given species X at a given time are defined in terms of the physical densities $\rho_X(a)$ via $\Omega_X(a) \equiv \rho_{\rm crit}^{-1}(a)\rho_X(a)$, where the critical density $\rho_{\rm crit}(a) = (8\pi G)^{-1}3H^2(a) = \rho_{\rm crit,0}H_0^{-2}H^2(a)$. As an example, the physical density of matter is given by $\rho_m(a) = \rho_{m,0}a^{-3} = \rho_{\rm crit,0}\Omega_{m,0}a^{-3}$, and its density parameter is $\Omega_m(a) = \Omega_{m,0}H_0^2 a^{-3}H^{-2}(a)$. CCL moreover allows for comoving physical densities $\rho_{X,\rm com}(a) = \rho_X(a)a^3$ to be extracted, which in the case of matter reduces to $\rho_{m,\rm com} = \rho_{\rm crit,0}\Omega_{m,0}$.

Fitting models to cosmological observables requires predicting cosmological distances for a given model. We consider the comoving radial distance, which is calculated via a numerical integral as

$$\chi(a) = c \int_a^1 \frac{da'}{a'^2 H(a')}. \qquad (4)$$

The comoving angular diameter distance is then computed in terms of the comoving radial distance,

$$r(\chi) = \begin{cases} k^{-1/2}\sin(k^{1/2}\chi) & k > 0 \\ \chi & k = 0 \\ |k|^{-1/2}\sinh(|k|^{1/2}\chi) & k < 0 \end{cases} \qquad (5)$$

where $k = \left(\sum_X \Omega_X - 1\right)c^{-2}H_0^2$ is the curvature. This function can be written directly in terms of the present curvature density parameter, $\Omega_{K,0}$, as

$$r(\chi) = \sqrt{\Omega_{K,0}}\sinh(\sqrt{\Omega_{K,0}}\chi), \qquad (6)$$

which is valid for all forms of the curvature density. The angular diameter distance is given by $d_A = a\,r(a)$, and the luminosity distance is $d_L = r(a)/a$, leading to the familiar relation $d_A = a^2 d_L$ which is valid in general for all metric theories of gravity. The CCL suite also has the functionality to compute the distance modulus, defined as

$$\mu = 5\log_{10}(d_L/\text{pc}) - 5, \qquad (7)$$

along with $a(\chi)$, the inverse function of $\chi(a)$.

2.2. *Growth of perturbations*

Volunteer(s) in charge: Mustapha Ishak **Once the 2 questions below are addressed this Sub-section is ready for review.**

Probing the growth history of the Universe can allow us to distinguish between cosmological models. To compute the linear growth factor of matter perturbations, $D(a)$, CCL solves the following differential equation:

$$\frac{d}{da}\left(a^3 H(a)\frac{dD}{da}\right) = \frac{3}{2}\Omega_M(a)aH(a)D, \qquad (8)$$

using a Runge-Kutta Cash-Karp algorithm.

In doing this, CCL simultaneously computes the logarithmic growth rate $f(a)$, defined as:

$$f(a) \equiv \frac{d\ln D}{d\ln a}. \qquad (9)$$

CCL provides functions that return the growth normalized to $D(a=1) = 1$ and to $D(a \ll 1) \to a$. It employs an accelerated spline that is linearly spaced in the scale factor to interpolate the growth functions.

The growth calculations cover flat and curved ΛCDM, wCDM, and $(w_0 + w_a)$CDM cosmologies. However, it should be noted that the above treatment is strictly valid for a Universe containing only dust-like matter components. A scale-independent growth rate is, for example, ill-defined in the presence of massive neutrinos; attempts to compute the growth rate in cosmologies with massive neutrinos will therefore fail by design. JAB: will CCL crash?

Finally, CCL allows for an alternative 'modified gravity' cosmological model defined by a regular background $(w_0 + w_a)$CDM (To do: with arbitrary K?) as well as a user-defined $\Delta f(a)$, such that the true growth rate in this model is given by $f(a) = f_0(a) + \Delta f(a)$, where $f_0(a)$ is the growth rate in the background model. Note that this model is only consistently implemented with regards to the computation of the linear growth factor and growth rates. All other CCL functions (including

the non-linear power spectrum) will ignore these modifications. This model, and the interpretation of the predictions given by `CCL`, should therefore be used with care. A version of the growth code and transfer functions depending on modified gravity parameters is under development.

2.3. *Matter power spectrum*

Volunteer(s) in charge: Elisa Chisari

Theoretical predictions for cosmological observables such as galaxy clustering, gravitational lensing and cluster mass functions rely on knowledge of the distribution of matter from small to large scales in the Universe. The quantity most frequently used to describe the distribution of matter at a given wavenumber and redshift is the matter power spectrum, $P(k,z)$, defined as

$$\langle \tilde{\delta}(\mathbf{k}, z)\tilde{\delta}(\mathbf{k}', z)\rangle = (2\pi)^3 P(k, z)\, \delta_D^3(\mathbf{k} - \mathbf{k}') \qquad (10)$$

where $\tilde{\delta}(\mathbf{k})$ is the Fourier component of the overdensity field at a given wavenumber and δ_D^3 is the Dirac delta function. $P(k,z)$ has units of volume and a dimensionless analogue is often defined as

$$\Delta^2(k, z) \equiv \frac{k^3}{2\pi^2} P(k, z). \qquad (11)$$

`CCL` implements several different methods for making predictions for the matter power spectrum. Two of those methods, the BBKS (Bardeen et al. 1986) and Eisenstein & Hu (1998) approximations, are only accurate to within a few percent and are implemented for validation purposes only. These approximations provide analytical expressions for the transfer function, $T(k)$, which is related to the matter power spectrum by $\Delta(k)^2 \propto T^2(k)k^{3+n_s}$, where n_s is the power-law index of the primordial power spectrum. The normalization of the power spectrum is either defined at $z = 0$ by setting σ_8 to its value today, or by setting the amplitude of primordial fluctuations, A_s.

The default `CCL` implementation uses the `CLASS` algorithm Blas et al. (2011) to obtain predictions for $P(k,z)$. In addition, `CCL` can also generate $P(k,z)$ predictions by emulation of cosmological numerical simuations, in particular, using the "Cosmic Emulator" developed by Lawrence et al. (2017).

None of the above methods account for the impact of baryonic physics on the distribution of matter, which is known to exceed percent level at scales $k \gtrsim 1/\text{Mpc}$ (van Daalen et al. 2011; Vogelsberger et al. 2014; Hellwing et al. 2016; Springel et al. 2017) and can affect the extraction of cosmological parameters (Semboloni et al. 2011, 2013; Mohammed & Seljak 2014; Eifler et al. 2015; Mohammed & Gnedin 2017). To account for this effect, we incorporate in `CCL` an effective parametrization

(Schneider & Teyssier 2015) of the redistribution of matter as a consequence of feedback from Active Galactic Nuclei and adiabatic cooling. We give an overview of each method to predict the matter power spectrum in what follows.

BBKS approximation. `CCL` implements the analytical BBKS approximation to the transfer function (Bardeen et al. 1986), given by

$$T\,(q \equiv k/\Gamma h \text{Mpc}^{-1}) = \frac{\ln[1 + 2.34q]}{2.34q} \times \qquad (12)$$
$$[1 + 3.89q + (16.2q)^2 + (5.47q)^3 + (6.71q)^4]^{-0.25}$$

where $\Gamma = \Omega_m h$. The BBKS power spectrum option is primarily used as a precisely-defined input for testing the numerical accuracy of `CCL` routines (as described in Sec. 3), and it is not recommended for other uses.

Eisenstein & Hu approximation. `CCL` also provides an approximation to the matter power spectrum as implemented by Eisenstein & Hu (1998) (we refer the reader to this paper for a detailed discussion of the fitting formulae).[2]

`CLASS`. The default configuration of `CCL` adopts predictions for the linear and nonlinear matter power spectrum from the publicly available software (Blas et al. 2011). `CLASS` currently computes the non-linear power spectrum using the HaloFit prescription of Takahashi et al. (2012).

Cosmic emulator. To do: In the section on the HMF and halo bias below, there is a lot of emphasis on the fact that these quantities are not themselves without significant uncertainty. Should we include a sentence or two to that effect here as well? - DL JAB: my general comment in the abstract is related to this. The emulator (Lawrence et al. 2017) provides accurate predictions for the nonlinear matter power spectrum, at the 1% level for $z \leq 2$ and in the wavenumber range $k = [10^{-3}, 5]$ Mpc^{-1}. The allowed range of cosmological parameters

---

[2] Note that the implementation in `CCL` modifies Eq. 5 of Eisenstein & Hu (1998) using $a^{-1} = 1 + z$ instead of the approximation $a^{-1} \sim z$. The difference in the resulting power spectra is negligible, but larger than 1 part in 10^4 for $k < 10\,h\,\text{Mpc}^{-1}$.

that can be passed to the emulator is as follows:

$$0.12 \leq \Omega_m h^2 \leq 0.155,$$
$$0.0215 \leq \Omega_b h^2 \leq 0.0235,$$
$$0.7 \leq \sigma_8 \leq 0.9,$$
$$0.55 \leq h \leq 0.85,$$
$$0.85 \leq n_s \leq 1.05,$$
$$-1.3 \leq w_0 \leq -0.7,$$
$$-1.73 \leq w_a \leq -0.7,\,[3]$$
$$0.0 \leq \Omega_{\nu,\mathrm{m}} h^2 \leq 0.01. \tag{13}$$

In the case of the emulator, the effective number of relativistic neutrino species is set to $N_{\mathrm{eff}} = 3.04$. In Lawrence et al. (2017), the neutrino component of the power spectrum is not simulated, but either linearly evolved and added to the simulated power spectra at low redshift, or accounted for by a scale-dependent correction to the growth function. More details on this method and its accuracy can be found in (Upadhye et al. 2014; Castorina et al. 2015; Heitmann et al. 2016).

Baryonic correction model (BCM). CCL incorporates the impact of baryons on the total matter power spectrum via the BCM of Schneider & Teyssier (2015). The main consequences of baryonic processes are: to suppress the power spectrum at intermediate scales ($k \sim$ a few h/Mpc) due to the ejection of gas by Active Galactic Nuclei feedback, and to enhance it at smaller scales due to adiabatic cooling. To account for these effects, BCM uses an effective decomposition for the impact of gas ejection (G) and the enhancement of the small scale profile due to star formation (S) to estimate the fractional effect of baryonic processes on the dark matter-only power spectrum (P_{DMO}):

$$P_{\mathrm{BCM}}(k,z) = P_{\mathrm{DMO}}(k,z) G(k|M_c, \eta_b, z) S(k|k_s) \tag{14}$$

Three effective parameters govern the contribution of baryonic processes to modifying the total matter power spectrum:

- $\log_{10}[M_c/(\mathrm{M}_\odot/h)]$: the mass of the clusters responsible for feedback, which regulates the amount of suppression of the matter power spectrum at intermediate scales;

- η_b: a dimensionless parameter which determines the scale at which suppression peaks;

- and k_s [h/Mpc]: the wavenumber that determines the scale of the stellar distribution of matter in the center of halos.

If these parameters are not specified by the user, CCL assumes the default parameters of Schneider & Teyssier (2015), calibrated through different comparisons with observations and simulations in that work.

2.4. *Two-point correlators*

Volunteer(s) in charge: David Alonso, Tom McClintock

This section describes the theoretical expectations for the two-point correlators of pairs of quantities (fields) defined on the sky. These fields can be classified in terms of their spin s under rotations on the plane tangent to the sphere. In general a spin-s field is defined by two real-valued functions of the spherical coordinates $a_1(\hat{\mathbf{n}})$ and $a_2(\hat{\mathbf{n}})$ (e.g. γ_1 and γ_2 for weak lensing or the Stokes parameters Q and U in the case of polarized intensity), from which one can form the complex field $a = a_1 + i a_2$.

Spin-s quantities can be decomposed into their harmonic coefficients $\,_s a_{\ell m}$ through a spherical harmonic transform:

$$_s a_{\ell m} = \int d\hat{\mathbf{n}}\, a(\hat{\mathbf{n}})\, _s Y^*_{\ell m}(\hat{\mathbf{n}}), \quad a(\hat{\mathbf{n}}) = \sum_{\ell m} {}_s a_{\ell m}\, Y_{\ell m}(\hat{\mathbf{n}})$$

where $\,_s Y_{\ell m}$ are the spin-weighed spherical harmonics. The harmonic coefficients can then be associated with parity-even and parity-odd components (E-modes and B-modes respectively) as[4]

$$E_{\ell m} = -\frac{1}{2} \left[_s a_{\ell m} + (-1)^s \,_{-s} a_{\ell m} \right]$$
$$i B_{\ell m} = -\frac{1}{2} \left[_s a_{\ell m} - (-1)^s \,_{-s} a_{\ell m} \right]$$

In what follows we will focus on scalar ($s = 0$) quantities such as the overdensity of source number counts or the lensing convergence, and on spin-2 fields such as the lensing shear. We will also distinguish between *tracers* (fields observed on the sky, such as number counts in a redshift bin, shear, or CMB temperature fluctuations) and *contributions* to the total observed fluctuations of these tracers (such as the biased matter density term in number counts, redshift-space distortions, magnification, etc.).

2.4.1. *Angular power spectra*

Volunteer(s) in charge: David Alonso

The angular power spectrum C^{ab}_ℓ between two tracers a and b is defined as

$$\langle a_{\ell m} b^*_{\ell m} \rangle \equiv C^{ab} \delta_{\ell \ell'} \delta_{m m'}, \tag{15}$$

where $a_{\ell m}$ and $b_{\ell m}$ can be either the E-mode or B-mode component of the corresponding field. In what follows

---

[4] We note that for spin-0 quantities the minus sign preceding these equations is usually omitted.

we will only deal with fields for which the B-modes are identically 0, and therefore all equations refer to the E-E power spectrum. In general, this power spectrum can be written as:

$$C_\ell^{ab} = 4\pi \int_0^\infty \frac{dk}{k}\, \mathcal{P}_\Phi(k)\Delta_\ell^a(k)\Delta_\ell^b(k), \qquad (16)$$

where $\mathcal{P}_\Phi(k)$ is the dimensionless power spectrum of the primordial curvature perturbations, and Δ^a and Δ^b are the transfer functions corresponding to these tracers. Each transfer function will receive contributions from different terms. Currently CCL supports three types of tracers: number counts, galaxy shape distortions and lensing convergence, with the following contributions:

Number counts. —The transfer function for number counts can be decomposed into three contributions: $\Delta^{\rm NC} = \Delta^{\rm D} + \Delta^{\rm RSD} + \Delta^{\rm M}$, where

- $\Delta^{\rm D}$ is the standard density term proportional to the matter density:

$$\Delta_\ell^{\rm D}(k) = \int dz\, p_z(z)\, b(z)\, T_\delta(k,z)\, j_\ell(k\chi(z)), \quad (17)$$

  where $j_\ell(x)$ is ℓ-th order spherical Bessel function, T_δ is the matter transfer function, $b(z)$ is the linear clustering bias for this tracer and $p_z(z)$ is the normalized distribution of sources in redshift (i.e. the selection function). The fluctuations in the number density of sources in different redshift bins are therefore treated by CCL as different tracers. Note that CCL currently does not support non-linear or scale-dependent bias, but future releases will do so under a number of schemes, including perturbative approaches as implemented in e.g. McEwen et al. (2016).

- $\Delta^{\rm RSD}$ is the linear contribution from redshift-space distortions (RSDs):

$$\Delta_\ell^{\rm RSD}(k) = \int dz\, \frac{(1+z)p_z(z)}{H(z)} T_\theta(k,z) j_\ell''(k\chi(z)), \tag{18}$$

  where $T_\theta(k,z)$ is the transfer function of θ, the divergence of the comoving velocity field, and j_ℓ'' is the second order derivative of the spherical Bessel function, j_ℓ. Note that the RSD contribution to number counts is currently computed by CCL assuming a linear-theory relation between the matter overdensity and peculiar velocity fields, mediated by the scale-independent growth rate f. While this should not be problematic for wide photometric redshift bins and standard cosmological

models, users should exercise care when interpreting results for narrow window functions or exotic cosmologies. Additionally, number count tracers with RSD in cosmologies with massive neutrinos are not currently supported.

- $\Delta^{\rm M}$ is the contribution from lensing magnification:

$$\Delta_\ell^{\rm M}(k) = -\ell(\ell+1)\int \frac{dz}{H(z)} W^{\rm M}(z)$$
$$T_{\phi+\psi}(k,z)j_\ell(k\chi(z)), \quad (19)$$

  where $T_{\phi+\psi}$ is the transfer function for the Newtonian-gauge scalar metric perturbations, and $W^{\rm M}$ is the magnification window function:

$$W^{\rm M}(z) \equiv \int_z^\infty dz'\, p_z(z')\frac{2-5s(z')}{2}\frac{r(\chi'-\chi)}{r(\chi')r(\chi)}. \tag{20}$$

  Here, $s(z)$ is the magnification bias, given as the logarithmic derivative of the number of sources with magnitude limit, and $r(\chi)$ is the angular comoving distance (see Eq. 5).

Note that CCL currently does not compute relativistic corrections to number counts (Challinor & Lewis 2011; Bonvin & Durrer 2011). Although these will be included in the future, their contribution to the total fluctuation is largely subdominant (see Alonso et al. (2015) and the two references above), and therefore it is safe to ignore them for our purposes.

Correlated galaxy shapes. —The transfer function for correlated galaxy shapes (intrinsic and lensed) is currently decomposed into two terms: $\Delta^{\rm SH} = \Delta^{\rm WL} + \Delta^{\rm IA}$, where

- $\Delta^{\rm L}$ is the standard lensing ("cosmic shear") contribution:

$$\Delta_\ell^{\rm L}(k) = -\frac{1}{2}\sqrt{\frac{(\ell+2)!}{(\ell-2)!}} \int \frac{dz}{H(z)} W^{\rm L}(z) T_{\phi+\psi}(k,z)$$
$$j_\ell(k\chi(z)), \qquad (21)$$

  where $W^{\rm L}$ is the lensing kernel, given by

$$W^L(z) \equiv \int_z^\infty dz' p_z(z')\frac{r(\chi'-\chi)}{r(\chi')r(\chi)}. \tag{22}$$

- $\Delta^{\rm IA}$ is the transfer function for intrinsic galaxy alignments. CCL currently supports the so-called "non-linear alignment model", in which the intrinsic galaxy inertia tensor is proportional the local tidal tensor Hirata & Seljak (2004); Hirata et al.

(2007):

$$\Delta_\ell^{\mathrm{IA}}(k) = \sqrt{\frac{(\ell+2)!}{(\ell-2)!}} \int dz\, p_z(z)\, b_{\mathrm{IA}}(z)\, f_{\mathrm{IA}}(z)$$

$$T_\delta(k,z)\, \frac{j_\ell(k\chi(z))}{[k\chi(z)]^2}. \quad (23)$$

Here, b_{IA} is the so-called alignment bias, and f_{IA} is the fraction of aligned galaxies in the sample. Notice that $b_{\mathrm{IA}}(z)$ absorbs the typical normalization factors used in the literature for intrinsic alignment amplitude and redshift evolution. It is thus not to be confused with C_1 or A_{IA}, typical parameters for the linear alignment model, as adopted in works such as Blazek et al. (2017); van Uitert et al. (2018); Joudaki et al. (2018); Hildebrandt et al. (2017).

Lensing convergence.—The transfer function for the lensing convergence of a given source plane at redshift z_* receives only one contribution, given by

$$\Delta_\ell^\kappa(k) = -\frac{\ell(\ell+1)}{2} \int_0^{\chi_*} \frac{dz}{H(z)} \frac{r(\chi_*-\chi)}{r(\chi)r(\chi_*)} T_{\phi+\psi}(k,z), \quad (24)$$

where $\chi_* \equiv \chi(z_*)$.

It is worth noting that the equations above should be modified for non-flat cosmologies by replacing the spherical Bessel functions j_ℓ with their hyperspherical counterparts (Kamionkowski & Spergel 1994). These are currently not supported by CCL To do: Clarify in Table 1?, and their impact is mostly relevant on low multipoles. The library also assumes a factorizable matter power spectrum at unequal times $P_\delta(k, z_1, z_2) = T_\delta(k, z_1) T_\delta(k, z_2)\, 2\pi^2 \mathcal{P}_\Phi(k)$ (see Kitching & Heavens 2017). Furthermore, CCL currently assumes a relation between transfer functions T_δ, T_θ and $T_{\phi+\psi}$ that is strictly only valid in vanilla ΛCDM:

$$T_\delta = -\frac{1+z}{H(z)f(z)} T_\theta = -\frac{k^2}{3H_0^2 \Omega_M} \frac{T_{\phi+\psi}}{1+z}. \quad (25)$$

These approximations will be revisited in future versions of the library. JAB: It appears we are defining the transfer function to include both the early universe physics and late-time nonlinear growth. Perhaps we should clarify this to avoid confusion with the standard linear theory transfer function.

2.4.2. Correlation functions

Volunteer(s) in charge: Elisa Chisari, Sukhdeep Singh

Fields can also be correlated in configuration space, and the corresponding correlators are called correlation functions. Let a and b be two fields with spins s_a and s_b. We start by defining $\tilde{a}(\hat{\mathbf{n}}_1)$ and $\tilde{b}(\hat{\mathbf{n}}_2)$ as the fields a and b rotated such that the x-axis of the tangential coordinate systems at $\hat{\mathbf{n}}_1$ and $\hat{\mathbf{n}}_2$ become aligned with the vector connecting both points. We can then define two correlation functions:

$$\xi_+^{ab}(\theta) \equiv \left\langle \tilde{a}(\hat{\mathbf{n}}_1)\tilde{b}^*(\hat{\mathbf{n}}_2) \right\rangle, \quad \xi_-^{ab}(\theta) \equiv \left\langle \tilde{a}(\hat{\mathbf{n}}_1)\tilde{b}(\hat{\mathbf{n}}_2) \right\rangle,$$

where $\hat{\mathbf{n}}_1 \cdot \hat{\mathbf{n}}_2 \equiv \cos\theta$.

$\xi_\pm$ can be related to the power spectra as

$$\xi_\pm^{ab} = \sum_\ell \frac{2\ell+1}{4\pi} (\pm1)^{s_b}\, C_\ell^{ab\pm}\, d_{s_a,\pm s_b}^\ell(\theta), \quad (26)$$

where $d_{mm'}^\ell$ are the Wigner-d matrices (Ng & Liu 1999; Chon et al. 2004) and we have defined the power spectra

$$C_\ell^{ab\pm} \equiv \left(C_\ell^{a_E b_E} \pm C_\ell^{a_B b_B} \right) + i \left(C_\ell^{a_B b_E} \pm C_\ell^{a_E b_B} \right), \quad (27)$$

which reduces to the EE power spectrum when all B-modes are 0.

Note that, as scalar quantities are real, any correlation involving at least one spin-0 field only has one non-unique correlation function. In these cases, the Wigner-d matrices can also be expressed in terms of associated Legendre polynomials P_ℓ^m, and therefore Eq. 26 becomes

$$\xi^{ab}(\theta) = \sum_\ell \frac{2\ell+1}{4\pi} C_\ell^{ab} \sqrt{\frac{(\ell-s_a)!}{(\ell+s_a)!}} P_\ell^{s_a}(\cos\theta) \quad (28)$$

$$= \sum_\ell \frac{2\ell+1}{4\pi} C_\ell^{ab} P_\ell(\cos\theta), \quad (29)$$

where the last equality holds for $s_a = 0$, and both expressions assume $s_b = 0$.

In the flat-sky approximation we can take the small-scale limit $\ell \gg s_1, s_2$ and approximate

$$d_{s_1 s_2}^\ell(\theta) \longrightarrow J_{s_1-s_2}(\ell\theta), \quad (30)$$

where $J_\alpha(x)$ is the Bessel function of order α. Eq. 26 then becomes[5]

$$\xi_\pm^{ab}(\theta) = (\pm1)^{s_b} \int \frac{d\ell\,\ell}{2\pi} C_\ell^{ab\pm} J_{s_a \mp s_b}(\ell\theta). \quad (31)$$

In summary, for spins 0 and 2, the three relevant cases for the cosmological observables supported by CCL are:

---

[5] See the weak lensing review by Bartelmann & Schneider (2001), page 44 and Joachimi & Bridle (2010).

- $s_a = s_b = 0$ (e.g. galaxy-galaxy, galaxy-κ and κ-κ):

$$\xi^{ab}(\theta) = \sum_\ell \frac{2\ell+1}{4\pi} C_\ell^{ab} P_\ell(\cos\theta) \quad \text{(full-sky)} \quad (32)$$

$$= \int_0^\infty \frac{d\ell\,\ell}{2\pi} C_\ell^{ab} J_0(\ell\theta) \qquad \text{(flat-sky)} \quad (33)$$

- $s_a = 2$, $s_b = 0$ (e.g. galaxy-shear, κ-shear):

$$\xi^{ab}(\theta) = \sum_\ell \frac{2\ell+1}{4\pi} C_\ell^{ab} d_{2,0}^\ell(\theta) \quad \text{(full-sky)} \quad (34)$$

$$= \int_0^\infty \frac{d\ell\,\ell}{2\pi} C_\ell^{ab} J_2(\ell\theta) \qquad \text{(flat-sky)} \quad (35)$$

- $s_a = s_b = 2$ (e.g. shear-shear):

$$\xi_\pm^{ab}(\theta) = \sum_\ell \frac{2\ell+1}{4\pi} C_\ell^{ab} d_{2,\pm2}^\ell(\theta) \quad \text{(full-sky)} \quad (36)$$

$$= \int_0^\infty \frac{d\ell\,\ell}{2\pi} C_\ell^{ab} J_{2\mp2}(\ell\theta) \qquad \text{(flat-sky)} \quad (37)$$

2.4.3. *3-dimensional spatial correlation function.*

In addition to the angular correlation functions, CCL can also be used to compute the three-dimensional spatial correlation function, $\xi(r)$, from the transform of the matter power spectrum:

$$\xi(r) = \frac{1}{2\pi^2} \int dk\, k^2 P(k) \frac{\sin(kr)}{kr} \qquad (38)$$

In the future CCL will be expanded to incorporate the calculation of the higher-order multipoles needed to characterize the redshift-space three-dimensional correlation function in the presence of RSDs.

2.5. *Halo mass function*

Volunteer(s) in charge: Antonio Villarreal, Tom McClintock

Being able to calculate the halo abundance as a function of mass is a necessary step to being able to constrain cosmology with probes such as galaxy clusters. While analytic functions are the traditional means of predicting evolution of halo abundances, calibration is frequently required against cosmological simulations. In order to reach the high precision required for cosmological constraints in a self-consistent fashion, it is ultimately necessary to use cosmological simulations; we implement this with halo mass functions with parameters fit to these simulations. The calculation of the halo mass function focuses around the spherical overdensity

method of halo finding, in which the size of a halo can be defined with:

$$\bar{\rho}(r_\Delta) = \Delta \times \bar{\rho}_{\rm m}, \qquad (39)$$

where a spherical halo with radius r_Δ has an average density $\bar{\rho}$ equal to the overdensity parameter Δ times the mean background density of the universe at a given redshift, $\bar{\rho}_{\rm m}(z)$. To do: I believe we use the same quantity without bars above. Make consistent? - DLASV: I would prefer the usage with bars throughout, as it is more explicit and matches uses in the simulation literature. Either direction I believe works though. Within the literature, the choice of Δ can vary considerably, as observations focusing on the compact cores of halos often take much larger values of Δ than the fiducial definition in most halo clustering studies, $\Delta = 200$. We note that another common definition exists which utilizes the critical density of the universe, $\rho_{\rm crit}$; this introduces a simple conversion factor between the two definitions that must be accounted for. Currently, CCL only accepts overdensity parameters with respect to the mean matter density, but we plan to allow for self-consistent handling of critical density based definitions in the future.

The halo mass function is defined as

$$\frac{dn}{dM} = f(\sigma) \frac{\bar{\rho}_{\rm m}}{M} \frac{d\ln\sigma^{-1}}{dM}, \qquad (40)$$

where n is the number density of halos of a given mass M associated with the RMS variance of the matter density field σ^2 at a given redshift and f is the derived fitting function[6]. To do: Clarify that this should not be confused with f the linear growth rate of structure as introduced above? - DL In CCL calling this function returns the mass function in logarithmic mass bins, $dn/d\log_{10} M$, where the input is the halo mass M and scale factor a.

The halo mass M is related to σ by first computing the radius R that would enclose a mass M in a homogeneous Universe at $z = 0$:

$$M = \frac{H_0^2}{2G} R^3 \rightarrow \frac{M}{M_\odot} = 1.162 \times 10^{12} \Omega_M h^2 \left(\frac{R}{1\,\text{Mpc}}\right)^3. \qquad (41)$$

The RMS density contrast in spheres of radius R can then be computed as

$$\sigma_R^2 = \frac{1}{2\pi^2} \int dk\, k^2\, P(k) \tilde{W}_R^2(k) \qquad (42)$$

where $P(k)$ is the linear matter power spectrum and $\tilde{W}(kR)$ is the Fourier transform of a spherical top hat

---

[6] Not to be confused with the linear growth rate of structure!

window function,

$$\tilde{W}_R(k) = \frac{3}{(kR)^3}[\sin(kR) - kR\cos(kR)]. \qquad (43)$$

This is commonly related in terms of the mass inside of the Lagrangian scale of the halo, using the following transformation:

$$R = (3M/4\pi\bar{\rho}_{\rm m})^{1/3}. \qquad (44)$$

As a consequence, one can also define σ_M as the RMS variance of the density field smoothed on some scale M, analogously to Eq.(42).

One commonly used halo mass function definition within the literature is the Tinker et al. (2010) fitting function. This fitting function has been developed using collisionless N-body simulation data, using halos identified by spherical overdensities. This is an extension of the Tinker et al. (2008) halo mass function, which is also included within CCL as a comparative option. This fitting function assumes little change with respect to cosmological parameters. Further, it includes a redshift scaling which is assumed to sharply end at a redshift of $z = 3$. This halo mass function is calibrated within the range of $10^{10.5}h{\rm M}_\odot \leq M \leq 10^{15.5}h{\rm M}_\odot$ at a redshift of $z = 0$.

For comparison purposes, we also have included the results of Angulo et al. (2012), which uses the Millenium XXL simulation in order to study galaxy cluster scaling relations. As part of this study, they have calculated their own fit to the Tinker et al. (2010) fitting function. While this additional halo mass function is available, it has not been extended to a broad range of overdensity parameter Δ, nor has it been extended beyond a redshift of $z = 0$.

The Tinker et al. (2008) fitting function uses the following parameterisation:

$$f(\sigma) = A\left[\left(\frac{\sigma}{b}\right)^{-a} + 1\right]e^{-c/\sigma^2}, \qquad (45)$$

where A, a, b, and c are fitting parameters that have additional redshift scaling. This basic form is modified for the Angulo et al. (2012) formulation. The resulting form is

$$f(\sigma) = A\left[\left(\frac{b}{\sigma} + 1\right)^{-a}\right]e^{-c/\sigma_M^2}, \qquad (46)$$

where the only change is in the formulation of the second term. Note that the fitting parameters in the Angulo et al. (2012) formulation do not contain any redshift dependence and the use of it is primarily for testing and benchmark purposes.

The Tinker et al. (2010) model parameterizes the halo mass function in terms of the peak height, $\nu = \delta_c/\sigma_M$,

where $\delta_c = 1.686$ is the critical density for collapse. The function is then re-expressed as

$$f(\nu) = \alpha[1 + (\beta\nu)^{-2\phi}]\nu^{2\eta}e(-\gamma\nu^2/2). \qquad (47)$$

We note that these halo mass functions, while implemented to high *numerical* accuracy through comparison against a flat ΛCDM cosmology (see 'CCL1' in Table 3), carry their own uncertainties. It has not been significantly studied whether the halo mass function is universal with respect to changes in dark energy parameterisation. Tinker et al. (2008, 2010) quote 5% accuracy of their mass funcitons. This result is consistent with the work of Watson et al. (2013), which also finds a 5% level difference in comparison to the Tinker fitting function. Further study will be required in the future in order to gain percent level accuracy in determining the halo mass function.To do: For what cosmologies was the Tinker mass function tested? I.e., what should go in Table 1?

2.6. *Halo bias*

Volunteer(s) in charge: Antonio Villarreal

JAB: I'm a bit confused by this section. This is a quantity that CCL can return. But currently the clustering observables can only handle linear (scale-independent) bias? And should we say that the user can specify a linear bias that does not come from this fitting formula? ASV: Including the Tinker fitting function for the halo bias is a fairly natural step considering we are also including the Tinker mass function (on which this is heavily related to). I do not think the fact that the clustering section of the code is currently unready to handle more than linear bias impacts the usefulness of having this built in. That being said, I will specify that currently we do not have a linear bias model built in as an explicit framework, though it can certainly be passed in to other sections of the code.

An important step in many interpretations of the halo model is to have a measure of the bias of dark matter halos, defined as the ratio of the halo power spectrum to the linear dark matter power spectrum,

$$b^2(k) = \frac{P_h(k)}{P_{\rm lin}(k)}. \qquad (48)$$

As with measures of the halo mass function, high accuracy cosmological constraints requires the use of numerical simulations to develop fitting functions and emulators. We note that we will define haloes as in the above subsection focusing on the halo mass function. CCL currently implements the halo bias fitting function results in Tinker et al. (2010), though future improvements will likely require the use of emulator methods.

The Tinker et al. (2010) model parameterizes the halo mass function and the halo bias in terms of the peak height and the critical density for collapse as

$$b(\nu) = 1 - A\frac{\nu^a}{\nu^a + \delta_c{}^a} + B\nu^b + C\nu^c, \qquad (49)$$

$$f(\nu) = \alpha[1 + (\beta\nu)^{-2\phi}]\nu^{2\eta}e(-\gamma\nu^2/2). \qquad (50)$$

Again, while high *numerical* accuracy has been verified, there is a remaining uncertainty. Tinker et al. (2010) found a $\sim 6\%$ scatter when determining the halo bias due to differences in simulations alone. In addition, this parameterization does not include a careful exploration of any impact due to changes in the dark energy equation of state. As with the halo mass function, studies will be required to reach accuracy at the percent level for any cosmological predictions.

We note that many observables are currently tuned to utilizing a linear halo bias (e.g. scale independent). While the current functionality of CCL is to return the Tinker et al. (2010) model for halo bias, it is entirely possible to generate simpler models of halo bias and pass this into further functions.

2.7. Halo model

Volunteer(s) in charge: Alexander Mead To do: This section will most likely be commented out.

In this section we review a basic halo-model computation (Seljak 2000; Peacock & Smith 2000; Cooray & Sheth 2002) of the cross-correlation between any two cosmological fields and only requires knowledge of the halo profiles of the field in question. For example, in the case of the matter-density auto spectrum we need only know the halo density profiles. For the galaxy spectrum we require knowledge of the number of, and distribution of, galaxies as a function of halo mass. In this simple form the halo model is approximate and makes the assumption that haloes are *linearly* biased with respect to the *linear* matter field and also assumes that haloes are spherical with properties that are determined solely by the halo mass. It is possible to go beyond these simplified assumptions, and we direct the interested reader to Cooray & Sheth (2002); Smith et al. (2007); Giocoli et al. (2010); Smith & Markovic (2011).

The eventual aim for CCL is to have a halo model that can calculate the auto- and cross-spectra for any cosmological field combinations with parameters that can be taken either from numerical simulations or observational data. Currently we have only implemented the case of the matter-density auto spectrum, but we keep the notation as general as possible in the following:

Consider two 3D cosmological fields ρ_i and ρ_j, the cross power spectrum at a given redshift can be written

as a sum of a two- and a one-halo term given by

$$P_{2\mathrm{H},ij}(k) = P_{\mathrm{lin}}(k) \prod_{n=i,j} \left[\int_0^\infty b(M)\frac{\mathrm{d}n}{\mathrm{d}M} W_n(M,k)\,\mathrm{d}M \right], \qquad (51)$$

$$P_{1\mathrm{H},ij}(k) = \int_0^\infty \frac{\mathrm{d}n}{\mathrm{d}M} W_i(M,k) W_j(M,k)\,\mathrm{d}M, \qquad (52)$$

where M is the halo mass, $\mathrm{d}n/\mathrm{d}M$ is the halo mass function defined in equation (40) and $b(M)$ is the linear halo bias with respect to the linear matter density field, defined as the large-scale limit of equation (48).

Equations (51) and (52) contain the (spherical) Fourier transform of the halo profile, or halo 'window function':

$$W_i(M,k) = \int_0^\infty 4\pi r^2 \frac{\sin(kr)}{kr}\rho_{\mathrm{H},i}(M,r)\,\mathrm{d}r, \qquad (53)$$

where $\rho_{\mathrm{H},i}(M,r)$ is the radial profile for the field i in a host halo of mass M. For example, if one is interested in matter fields then this would be the halo density profile, if one were interested in galaxies then this would be the number density and distribution of galaxies around a halo of mass M.

Note that the halo mass function and bias *must* satisfy the following properties for the total power spectrum to have the correct large-scale limit[7]:

$$\frac{1}{\bar{\rho}_{\mathrm{m}}} \int_0^\infty M\frac{\mathrm{d}n}{\mathrm{d}M}\,\mathrm{d}M = 1, \qquad (54)$$

$$\frac{1}{\bar{\rho}_{\mathrm{m}}} \int_0^\infty Mb(M)\frac{\mathrm{d}n}{\mathrm{d}M}\,\mathrm{d}M = 1. \qquad (55)$$

If one uses a mass function and bias pair that are related via the peak-background split formalism (Mo & White 1996; Sheth et al. 2001) the these conditions are automatically satisfied. In words these equations enforce that all matter is associated to a halo and that matter is on average unbiased with respect to itself. In the convention used in CCL the units of $P(k)$ will be exactly the units of $\rho_i\rho_j/\mathrm{Mpc}^3$. The units of the W_i are those of ρ_i multiplied by volume.

For the matter power spectrum we use the halo profiles of Navarro, Frenk, & White (NFW; 1997):

$$\rho_{\mathrm{H}}(M,r) \propto \frac{1}{r/r_{\mathrm{s}}(1 + r/r_{\mathrm{s}})^2}, \qquad (56)$$

---

[7] Note that achieving these correct limits for some fields is difficult numerically because of the large amount of mass contained in low mass haloes according to most popular mass functions. Special care must be taken with the two-halo integral in the case of matter power spectra.

which is written in terms of a scale radius r_s. The constant of proportionality fixed by the condition that the halo has total mass M when the boundary is set at the virial radius r_v, which is set such that the halo has a fixed density Δ_v with respect to the mean

$$M = 4\pi r_v^3 \Delta_v \bar{\rho} \ . \tag{57}$$

Finally, the scale radius is usually expressed in terms of the mass-dependent halo concentration parameter $c(M) = r_v/r_s$. We use the simple mass-concentration relation from Bullock et al. (2001)

$$c(M) = 9 \left(\frac{M}{M_*} \right)^{-0.13} \ , \tag{58}$$

where $\delta_c/\sigma(M_*) = 1$. Note that, in order to be consistent, one should use a value of Δ_v and $c(M)$ that is consistent with the halo definition used for the halo mass function and bias.

2.8. Photometric redshifts

Volunteer(s) in charge: Danielle Leonard **Section ready for revision**

Redshifts of LSST galaxies will be obtained via photometry. Therefore, performing any cosmological analysis which incorporates redshift information requires a model for the probability of measuring a photometric redshift z_{ph} for an object with hypothetical spectroscopic redshift z_s. In order to maintain agnosticism towards the optimal model, and hence to allow for the future inclusion of advancements from ongoing research, CCL allows the user to flexibly input a photometric redshift model. In addition, for ease of use, CCL provides the option of using a built-in function for a simple Gaussian photometric redshift probability distribution. The photometric redshift model can then be used, for example, when computing $\frac{dN}{dz}^i$ in photometric redshift bin i, as given by:

$$\frac{dN}{dz}^i = \frac{\frac{dN}{dz} \int_{z_i}^{z_{i+1}} dz' p(z, z')}{\int_{z_{min}}^{z_{max}} dz \frac{dN}{dz} \int_{z_i}^{z_{i+1}} dz' p(z, z')} \tag{59}$$

where $p(z, z')$ is the photometric redshift probability distribution, and z_i and z_{i+1} are the photo-z edges of the bin in question. In the case of the simple Gaussian photometric redshift model for which support is included in CCL out of the box, $p(z, z')$ is given as

$$p(z, z') = \frac{1}{\sqrt{2\pi}\sigma_z} \exp\left(-\frac{(z - z')^2}{2\sigma_z^2} \right). \tag{60}$$

3. IMPLEMENTATION OF HIGH-ACCURACY COSMOLOGICAL FUNCTIONS

Section ready for revision
In this section, we note some of the assumptions and implementation details that are relevant when making accurate cosmological predictions. The validation tests performed for CCL are described in detail in Section 4.

3.1. Background functions & growth of perturbations

Volunteer(s) in charge: Mustapha Ishak **Once we agree on the last paragraph, this Sub-section is ready for review.**

Cosmological predictions require making assumptions on the values of several physical constants, as defined in the previous sections. We have performed a comparison of the physical constants used in CCL to those used in GSL and CLASS as well as published sources such as the NIST Handbook and PDG Review of Particle Physics (Beringer et al. 2012). Where possible, we have set constants to the values that are used internally in CLASS. This includes the value of the gravitational constant, the Boltzmann constant, the Planck constant, the speed of light, and the electron charge. CLASS does not include a definition of the solar mass or the Stefan-Boltzmann constant so we use the values used by GSL. After comparison between the physical constants used in CCL and those of the sources mentioned above, we have found better than 10^{-4} agreement with everything except the gravitational constant.

The value of the gravitational constant, G, enters into the critical density. We found that failure to define G with sufficient precision initially resulted in lack of convergence at the 10^{-4} level between the CCL outputs and benchmarks (and among benchmarks). Importantly, note that CAMB barely has 10^{-4} precision in G (and similarly, there might be other constants within CAMB/CLASS for which one should check the precision level). For CCL predictions and benchmarks To do: Was this the G we used for benchmarks?, we are using the value from CLASS.MI: We should agree on how to revise this last paragraph.

3.2. Matter power spectrum

Volunteer(s) in charge: Elisa Chisari, Christiane Lorenz

For speed, the initialization of a cosmological model within CCL performs initial computations of the linear and nonlinear matter power spectra, which are then interpolated whenever required. The spline is performed in two variables: the logarithmically-spaced wavenumber and the logarithmically and linearly-spaced scale factor. Splining the power spectra output leads to some precision loss (compared to, for example, direct outputs from CLASS or the cosmic emulator) which is quantified in Section 4.

We introduce a maximum value k (in units of 1/Mpc) up to which we evaluate the power spectra for interpolation; we call this parameter `K_MAX_SPLINE`. A separate `K_MAX` parameter sets the limit of evaluation of the matter power spectrum. The range between `K_MAX_SPLINE` $< k <$ `K_MAX` is evaluated by performing a second order Taylor expansion in $\ln k$.

The Taylor expansion is implemented as follows: first, we compute the first and second derivative of $\ln P(k,z)$ at $k_0 = $ `K_MAX` $- 2\Delta \ln k$ via finite difference derivatives using `GSL`. The fiducial choice for $\Delta \ln k$ is 10^{-2}. We then apply a second order Taylor expansion to extrapolate the matter power spectrum to $k > $ `K_MAX_SPLINE`. The Taylor expansion gives

$$\ln P(k,z) \simeq \ln P(k_0,z) + \frac{d \ln P}{d \ln k}(\ln k_0, z)(\ln k - \ln k_0)$$
$$+ \frac{1}{2} \frac{d^2 \ln P}{d \ln k^2}(\ln k_0, z)(\ln k - \ln k_0)^2. \quad (61)$$

We also extrapolate the power spectrum at small wavenumbers. In this case, we introduce the parameter `K_MIN`, the wavenumber below which the power spectra are obtained by a power-law extrapolation with index n_s:

$$\log P(k < \text{K\_MIN}, z) = \log P(\text{K\_MIN}, z) + n_s(\log k - \log \text{K\_MIN}) \quad (62)$$

The value adopted for `K_MIN` depends on the choice of power spectrum method. Note that an additional parameter, `K_MIN_DEFAULT`, sets the minimum k for integrations. This is set to `K_MIN_DEFAULT` $= 5 \times 10^{-5}$/Mpc. For `CLASS` and the nonlinear power spectrum, we adopt `K_MIN` that coincides with the smallest wavenumber output by CLASS, `K_MIN` $= 7 \times 10^{-6}$/Mpc.[8] As a consequence, when using `CCL` with `CLASS`, no extrapolation will occur at low wavenumbers unless the user modified the default values of `K_MIN_DEFAULT` and/or `K_MIN` .

3.3. *Angular power spectra*

Volunteer(s) in charge: David Alonso

Different numerical approaches have been implemented in the library in order to expedite the computation of angular power spectra. We describe these here.

3.3.1. *Limber approximation*

Volunteer(s) in charge: David Alonso, Jérémy Neveu

---

[8] For BBKS, the power spectrum is computed analytically at all k, i.e., there is no extrapolation. For the Eisenstein & Hu implementation, the splines of the power spectrum span `K_MIN_DEFAULT`$< k <$`K_MAX_SPLINE`, so there is only extrapolation at high k.

As shown in Section 2.4.1, computing each transfer function contributing to a given power spectrum involves a radial projection (i.e. an integral over redshift or z or χ), and thus computing full power spectra consists of a triple integral for each ℓ. This can be computationally intensive, but can be significantly simplified in certain regimes by using the Limber approximation, given by:

$$j_\ell(x) \simeq \sqrt{\frac{\pi}{2\ell+1}} \, \delta\left(\ell + \frac{1}{2} - x\right). \quad (63)$$

This eliminates the integrals associated with each of the two transfer functions, massively accelerating the calculation.

Thus for each k and ℓ we can define a radial distance $\chi_\ell \equiv (\ell+1/2)/k$, with corresponding redshift z_ℓ. Substituting this in the expressions presented in Section 2.4.1, the power spectrum can be computed as a single integral:

$$C_\ell^{ab} = \frac{2}{2\ell+1} \int_0^\infty dk \, P_\delta(k, z_\ell) \tilde{\Delta}_\ell^a(k) \tilde{\Delta}_\ell^b(k). \quad (64)$$

where

$$\tilde{\Delta}_\ell^{\mathrm{D}}(k) = p_z(z_\ell) \, b(z_\ell) \, H(z_\ell) \quad (65)$$

$$\tilde{\Delta}_\ell^{\mathrm{RSD}}(k) = \frac{1+8\ell}{(2\ell+1)^2} \, p_z(z_\ell) \, f(z_\ell) \, H(z_\ell) - \quad (66)$$

$$\frac{4}{2\ell+3}\sqrt{\frac{2\ell+1}{2\ell+3}} p_z(z_{\ell+1}) \, f(z_{\ell+1}) \, H(z_{\ell+1})$$

$$\tilde{\Delta}_\ell^{\mathrm{M}}(k) = 3\Omega_{M,0}H_0^2 \frac{\ell(\ell+1)}{k^2} \frac{(1+z_\ell)}{\chi_\ell} W^{\mathrm{M}}(z_\ell) \quad (67)$$

$$\tilde{\Delta}_\ell^{\mathrm{L}}(k) = \frac{3}{2}\Omega_{M,0}H_0^2 \sqrt{\frac{(\ell+2)!}{(\ell-2)}} \frac{1}{k^2} \frac{1+z_\ell}{\chi_\ell} W^{\mathrm{L}}(z_\ell) \quad (68)$$

$$\tilde{\Delta}_\ell^{\mathrm{IA}}(k) = \sqrt{\frac{(\ell+2)!}{(\ell-2)!}} \frac{p_z(z_\ell) \, b_{\mathrm{IA}}(z_\ell) f_{\mathrm{red}}(z_\ell) H(z_\ell)}{(\ell+1/2)^2}. \quad (69)$$

The Limber approximation works best for wide radial kernels and high ℓ.

3.3.2. *Beyond Limber: Angpow*

Volunteer(s) in charge: Jérémy Neveu

`CCL` incorporates natively routines to compute the C_ℓ^{ab} angular power spectra as described above without the Limber approximation. The algorithm performs first the integrals over z for both tracers, and ends with the k integral. This computation is much slower than using the Limber approximation, but results in precise angular power spectra at low ℓ, and correct cross-correlations between tracers. Indeed as the Limber approximation consists in replacing oscillatory functions by Dirac distributions, the latter fails at reproducing the beat phenomenon $j_\ell(x) \times j_\ell(x')$ appearing when two oscillatory

functions are multiplied. The integration of these routines has been tested against the `CLASS` code and recovers the same angular power spectra when precision parameters are set to high values.

However, the computation of the C_ℓ^{ab} without the Limber approximation is too costly in terms of computing time using this method, if one wants to explore extensively a full cosmological parameter space. The aim of the `Angpow` software (Campagne et al. 2017a) is to compute the angular power spectra C_ℓ^{ab} without any Limber numerical approximation in a faster way but still accurately. `CCL` has been linked to the `Angpow` code, which is briefly described here.

The angular power spectrum for two tracers C_ℓ^{ab} is computed in `Angpow` according to the following expression

$$C_\ell^{ab} = \iint_0^\infty \mathrm{d}z\mathrm{d}z' p_{z_1}(z_1) p_{z_2}(z') \times \int_0^\infty \mathrm{d}k\, f_\ell(z,k) f_\ell(z',k). \tag{70}$$

The auxiliary function $f_\ell(z,k)$ can be defined without loss of generality as

$$f_\ell(z,k) \equiv \sqrt{\frac{2}{\pi}}\, k \sqrt{P_\delta(k,z)}\, \widetilde{\Delta}_\ell(z,k) \tag{71}$$

with $\widetilde{\Delta}_\ell(z,k)$ the function describing the physical processes such as matter density fluctuations, redshift-space distortions as described for instance in references Durrer (2008); Yoo et al. (2009); Yoo (2010); Challinor & Lewis (2011); Bonvin & Durrer (2011). Currently, the `Angpow` version delivered with `CCL` can only deal with galaxy clustering tracers (no lensing), and this without the magnification lensing term (equation 19). The plug in of those transfer functions is left for future work. For now, for galaxy clustering tracers we define $\widetilde{\Delta}_\ell(z,k)$ as

$$\widetilde{\Delta}_\ell(z,k) \approx b(z) j_\ell(k\chi(z)) - f(z) j''_\ell(k\chi(z)) \tag{72}$$

with $j_\ell(x)$ and $j''_\ell(x)$ the spherical Bessel function of order ℓ and its second derivative, and $f(z)$ the growth rate of structure.

In `Angpow`, the inner integral in k is computed first. To conduct the computation of such an integral of highly oscillating functions, the 3C-algorithm described in details in (Campagne et al. 2017a) is used. In brief, it relies on the projection of the oscillating $f_\ell(z,k)$ onto a Chebyshev series of order 2^N, the product of the two Chebyshev series is performed with a 2^{2N} Chebyshev series; then the integral is computed using Clenshaw-Curtis quadrature. Finally, the integrals over z are performed via again an optimised Clenshaw-Curtis quadrature. All the Chebyshev expansions and the Clenshaw-Curtis quadrature are performed via the *Discrete Cosine*

Transform of type I from the DCT-I fast transform of the FFTW library (Frigo & Johnson 2012).

As in the general case the Limber approximation is valid at high ℓ values, the `CCL` user can define an ℓ threshold to switch from the non-Limber slow computation to the faster Limber approximation.

3.4. *Correlation functions*

Volunteer(s) in charge: Elisa Chisari, Sukhdeep Singh

The exact Equations (32, 34, 36) relating the angular correlation functions and power spectra involve carrying out $N_\theta \times \ell_{max}$ operations, where $\ell_{max} \sim O(10^{4-5})$ is the maximum multipole needed to achieve convergence and N_θ is the number of angular scales θ at which the angular correlation function needs to be computed. Thus, evaluating these expressions directly becomes prohibitively slow and should be avoided except in regimes where other approximations are not valid. In particular `CCL` only supports the brute-force evaluation of these equations for correlations involving at least one spin-0 field. The currently preferred method in `CCL` is to use the flat-sky approximation and evaluate the Hankel transforms (Eqs. 33, 35, 37).

`CCL` currently provides two methods to compute Hankel transforms:

- **Brute-force integration.** `CCL` allows users to compute Hankel transforms by brute-force integration over the Bessel functions. The oscillating nature of these functions makes this method slow and not appropriate for likelihood-sampling. The preferred method to compute correlation functions is through the use of `FFTlog` (see below), and we support the brute-force method only for testing and validation.

- **FFTlog.** The public code `FFTlog`[9] is able to compute fast Hankel transforms through the assumption that the kernels of these transforms are periodic functions in logarithmic space. The Hankel transform can then be solved using Fast Fourier Transforms at a much lower computational expense than brute-force integration (Hamilton 2000; Talman 2009). `CCL` incorporates a version of the `FFTlog` method with only minor modifications from the original. The only potential drawback of this methods is the need to sample the kernels (i.e. the C_ℓ) on very small scales to ensure the convergence of the method. To do this, `CCL` extrapolates the power spectrum as a power law ($C_\ell \propto \ell^\beta$) To

---

[9] http://casa.colorado.edu/~ajsh/FFTLog/

We should also note that other approaches relating the correlation functions directly with the 3D matter power spectrum (e.g. Campagne et al. 2017b) could be useful in accelerating this computation, and we will explore these avenues in the future.

3.5. *Halo mass function*

To achieve 10^{-4} precision in $\sigma(M)$ and the normalisation of the power spectrum, one should check that the integral of σ_8 and $\sigma(M)$ has converged for the chosen values of $\{k_{\min}, k_{\max}\}$. After checking convergence, we achieved the desired precision.

Also note that for $\sigma(M)$, it is important to set the desired precision level correctly for the numerical integrator. The integral usually yields $\sigma^2(M)$, and not $\sigma(M)$. Hence, one has to set the desired precision taking the exponent into account.

Derivatives are calculated utilizing a spline that is built off of the previously described $\sigma(M)$ spline. As such, these splines cover the range from 10^6 to $10^{17} M_\odot$. For each value of $\log(M)$ in our spline evaluation, we calculate the value of $\sigma(M)$ half a step in either direction. We use the difference compared to the mass spacing to calculate an approximate derivative, which is then used in the spline interpolation. This has been tested to meet our necessary precision for the halo mass function within the mass range explored by Tinker et al. (2010). We note that there the accuracy is reduced at the edges of these splines and exploring extreme mass ranges may require changes in the parameters to initialize these splines.

In order to accomodate a wide range of values of the overdensity parameter Δ, we have generated a spline interpolation between best fit values as defined by Tinker et al. (2008) and Tinker et al. (2010). This covers a dynamic range from $\Delta = 200$ to 3200. Within this range, we interpolate in the space of the fit parameter and $\log \Delta$ using the Akima interpolation built from piecewise third order polynomials. We have chosen this rather than the fitting formulas utilized in Tinker et al. (2010) in order to assure high precision match to the Tinker halo mass function when choosing a value of Δ directly from the paper.

3.6. *Massive neutrinos*

When initializing a cosmology with massive neutrinos within CCL, the user can provide either a single value for m_ν, corresponding to a sum of the masses of three neutrinos, or a set of three values, corresponding directly to the three masses. In the former case, one can also specify how the sum of masses should be split for calculations. The default behavior of CCL is to split the sum into three masses which are consistent with the normal neutrinio mass hierarchy, but an inverted hierarchy or equal splitting can be requested. (For a review of the neutrino mass hierarchies and relevant particle physics results, see for example Lattanzi & Gerbino (2017); Lesgourgues & Pastor (2012).)

For equal splitting, it is clearly trivial to compute the three neutrino masses. If splitting with respect to the normal or inverted hierarchy is desired, it is slightly more complicated. The relevant known quantity which has been determined via particle physics experiments is the square of the difference of neutrino masses (up to a sign for one of the differences, hence the two possible hierarchies). Because we know the square of the differences rather than the differences themselves, we must solve a set of quadratic equations for the neutrino masses. In CCL this is accomplished by making use the knowledge that the mass difference between two of the neutrino species is small. This allows us to Taylor expand about this difference, and greatly simplifies solving for the three neutrino masses. This methodology represents an approximation (related to discarding higher-order terms in this Taylor expansion), however it produces discrepancies from the exact solution which result in cosmological predictions which differ at levels far below our required validation levels (detailed below in Section 4).

Having then a set of three neutrino masses, we check which of the corresponding neutrino species is non-relativistic today ($m_\nu > 0.00017$, Lesgourgues & Pastor 2012), and obtain the number of massive neutrinos in the cosmology. We use this, along with $N_{\rm eff}$, to set the number of relativistic neutrinos species, which is required in computing Ω_g and $\Omega_{\nu,\rm rel}$. We must be slightly careful in doing so, as for massive neutrinos only we modify the relationship between the temperature of the CMB and the neutrino temperature as described below equation 3 above. In order to compute $N_{\nu,\rm rel}$ consistent with the $N_{\rm eff}$ passed by the user, we do:

$$N_{\nu,\rm rel} = N_{\rm eff} - (T_{\rm NCDM})^4 \left(\frac{4}{11} \right)^{-\frac{4}{3}} N_{\nu,\rm m}. \qquad (73)$$

It may sometimes be preferable or necessarily to specify a cosmology in terms of $\Omega_{\nu,m}$ instead of m_ν. To facilitate this, `CCL` includes a convenience function which returns the latter given the former.

In equation 3 above, we specify how $\Omega_{\nu,m}$ is computed for a given cosmology with massive neutrinos. Within this expression is a phase-space integral:

$$\int_0^\infty dx\, x^2 \frac{\sqrt{x^2 + (\mu)^2}}{\exp(x) + 1}. \tag{74}$$

At high and low μ, corresponding to high and low mass neutrinos, this integral need not be evaluated numerically. At high μ, we set the integral equal to $\frac{5\zeta(3)}{18\pi^4}\mu$, while at low μ it goes to $\frac{7}{8}$. The μ values at which these approximations are taken can be set by the user. Outside of the regime in which these approximations are valid, the integral is computed numerically using `gsl`, splined, and stored such that for a single cosmology it must only be computed once.

4. VALIDATION OVER THE ΛCDM PARAMETER SPACE

Volunteer(s) in charge: Elisa Chisari, Antonio Villarreal, Phil Bull, Elisabeth Krause

Suggested content: Overview of the code comparison. How the codes used for comparison were selected. Validation plots for several observables.

Our goal in building `CCL` was to ensure that all outputs are validated to a well established accuracy level. This was achieved by comparing these outputs against one or multiple independent benchmarks obtained in the same configuration (i.e., for the same cosmology). In this section we document the accuracy achieved for each observable. In some cases, the achieved level of accuracy is higher than the impact of other systematics which have not yet been considered in this version of `CCL`. To do: Not sure what this previous sentence refers to. In the cases where this applies, we make it clear below. Table 2 summarises all the `CCL` validation tests discussed in this section.

`CCL` benchmarks are available and documented through the code repository. All plots presented in this section can be reproduced by means of a `python` notebook available with the code. Accuracy checks can also be run automatically upon installation of the software.

4.1. *Background quantities & growth of perturbations*

Comoving radial distances, the growth factor and distance moduli were compared against independently produced benchmarks at a set of low, $z = 0, 1, 2, 3, 4, 5$, and high redshifts, $10 \leq z \leq 10^3$. These comparisons were performed for the cosmologies listed in Table 3. The target level of accuracy was 10^{-4} and this was achieved or surpassed for all the background quantities. Figure 2 summarizes our results for cosmologies without massive neutrinos. The left panels show the distance accuracy achieved for different cosmological models (curves of different thickness) as a function of redshift, which is always better than 10^{-6}. Similarly, the right panels show the growth factor accuracy, which is $< 10^{-5}$.

Analogous comparisons of the comoving radial distances were made to independently produced benchmarks at low and high redshifts for cosmologies containing massive neutrinos. (Notice that the growth function with massive neutrinos is not supported by `CCL` because it is scale-dependent and therefore ill defined in our current framework.) These comparisons are displayed in Figure 3. The cosmological models used in tests of background quantities for cosmologies with massive neutrinos are given in Table 4. In this case, the benchmarks were produced by the `astropy` library (Astropy Collaboration et al. 2013). We increase the maximum tolerated fractional difference between quantities produced by `CCL` and benchmarks in this case to 10^{-3}, due to the fact that while `CCL` uses the full phase-space integral in computing the massive neutrino density as defined above, `astropy` uses a fitting function which is itself not accurate at a 10^{-3} level. As can be seen in Table 4, we perform comparisons in cosmologies with $N_{eff} = 3$ rather than the more standard $N_{eff} = 3.046$ in order to ensure the same cosmologies can easily be defined in `CCL` and `astropy` To do: Tilman, add comments on CLASS-based neutrino tests when merged.

4.2. *Matter power spectra*
4.2.1. *Analytic expressions*

Volunteer(s) in charge: Elisa Chisari

As discussed in Section 2.3, several power spectrum methods are implemented in `CCL`. Two of them, the BBKS (Bardeen et al. 1986) and the Eisenstein & Hu methods are implemented for validation purposes only and feed into the tests for observables such as angular power spectra and correlation functions, as we will see in subsequent sections. These two implementations have been validated against independent implementations. For BBKS, this test was performed at $0 \leq z \leq 5$ in the wavenumber range $10^{-3} \leq k \leq 10h/\mathrm{Mpc}$ with 10 bins per decade, and yielded an accuracy level of 10^{-4}. [10] For the Eisenstein & Hu matter power spec-

---

[10] We noticed that there are 2 typographical errors for the BBKS transfer function in "Modern Cosmology" (Dodelson 2004) compared to the original BBKS paper. The quadratic term should

Quantity	Equation/Reference	Cosmologies	Range	Accuracy
Comoving radial distance (low z)	(4)	CCL1-5	$0 \le z \le 5$	10^{-4}
Comoving radial distance (high z)	(4)	CCL1-3	$10 \le z \le 10^3$	10^{-4}
Growth (low z)	(8)	CCL1-5	$0 \le z \le 5$	10^{-4}
Growth (high z)	(8)	CCL1-3	$10 \le z \le 10^3$	10^{-4}
$\sigma(M)$ (BBKS)	(42)	CCL1-3	$10^6 \le M/(\mathrm{M}_\odot/h) \le 10^{16}$	10^{-4}
dn/dM	(40)	CCL1	$10^{10} \le M/(\mathrm{M}_\odot) \le 10^{16}$ & $z=0$	5×10^{-3}
$P(k)$ (BBKS)	(12)	CCL1-3	$10^{-3} \le k/(h/\mathrm{Mpc}) \le 10$ & $0 \le z \le 5$	10^{-4}
$P(k)$ (Eisenstein & Hu)	Eisenstein & Hu (1998)	CCL1	$10^{-3} \le k/(h/\mathrm{Mpc}) \le 10$ & $0 \le z \le 5$	10^{-4}
$P(k)$ (CosmicEmu wCDM)	Lawrence et al. (2017)	M1,M3,M5,M6,M8,M10	$10^{-3} \le k/\mathrm{Mpc}^{-1} \le 5$ & $z=0$	3×10^{-2}
$P(k)$ (CosmicEmu νCDM)	Lawrence et al. (2017)	M38,M39,M40,M42	$10^{-3} \le k/\mathrm{Mpc}^{-1} \le 5$ & $z=0$	3×10^{-2}
C_ℓ clustering	(16),(17)	CCL6	$1 \le l \le 30000$	10^{-3}
C_ℓ weak lensing	(16),(21)	CCL6	$1 \le l \le 30000$	10^{-3}
C_ℓ CMB lensing	(16),(24)	CCL6	$1 \le l \le 3000$	3×10^{-3}
ξ_+, ξ_-, ξ	(37),(33)	CCL6	$0.01 < \theta/\mathrm{deg} < 5$	0.5σ
3D correlation	(38)	CCL1-5	$1 < r/\mathrm{Mpc} < 200$ & $0 \le z \le 5$	4×10^{-3}
C_ℓ clustering non-Limber	(16),(17),(18)	CCL1	$500 \le l < 1000$	2×10^{-2}
C_ℓ clustering Angpow	(16),(17),(18)	CCL1	$1 \le l < 1000$	1×10^{-2}

To do: CLASS?

Cosmological models for code comparison project									
Acronym	Model	Ω_m	Ω_b	Ω_Λ	h_0	σ_8	n_s	w_0	w_a
CCL1	flat ΛCDM	0.3	0.05	0.7	0.7	0.8	0.96	-1	0
CCL2	w_0 ΛCDM	0.3	0.05	0.7	0.7	0.8	0.96	-0.9	0
CCL3	w_a ΛCDM	0.3	0.05	0.7	0.7	0.8	0.96	-0.9	0.1
CCL4	open w_a ΛCDM	0.3	0.05	0.65	0.7	0.8	0.96	-0.9	0.1
CCL5	closed w_a ΛCDM	0.3	0.05	0.75	0.7	0.8	0.96	-0.9	0.1
CCL6	flat ΛCDM	0.3	0	0.7	0.7	0.8	0.96	-1	0

Table 3. Cosmological models for code comparison project. To do: Model 6 was introduced because we use it in some of the checks, it needs more explanation in the main text
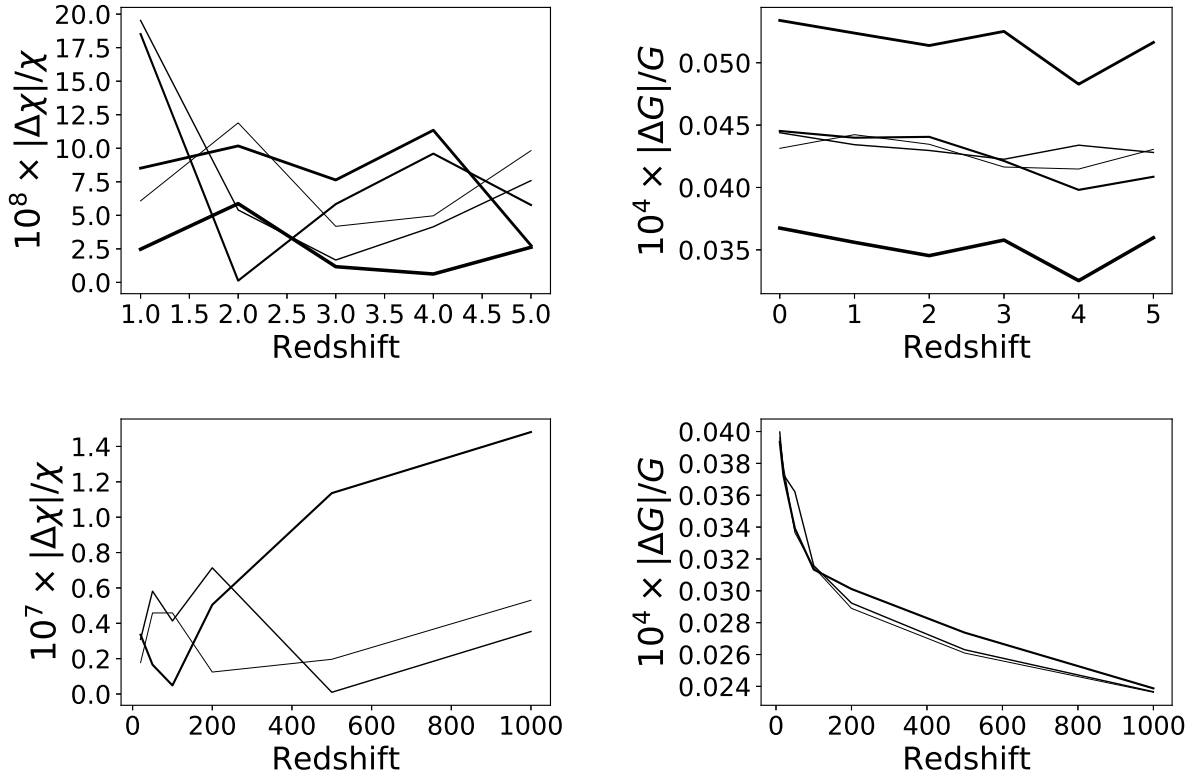
Figure 2. Accuracy achieved by `CCL` in the prediction of distances (left panels) and growth factor (right panels) for models CCL1-5 documented in Table 3. Different models correspond to different thickness curves. The top panels represent the accuracy checks at low redshift, while the bottom panels demonstrate accuracy up to high redshift.

Cosmological models with massive neutrinos										
Acronym	Model	Ω_m	Ω_b	Ω_Λ	h_0	σ_8	n_s	w_0	w_a	N_{eff}	m_ν (eV)
CCL7	flat ΛCDM, m_ν	0.3	0.05	0.7	0.7	0.8	0.96	-1	0	3	{0.04, 0, 0}
CCL8	w_0 ΛCDM, m_ν	0.3	0.05	0.7	0.7	0.8	0.96	-0.9	0	3	{0.05, 0.01, }
CCL9	w_a ΛCDM, m_ν	0.3	0.05	0.7	0.7	0.8	0.96	-0.9	0.1	3	{0.03, 0.02, 0.04}
CCL10	open w_a ΛCDM, m_ν	0.3	0.05	0.65	0.7	0.8	0.96	-0.9	0.1	3	{0.05, 0, 0}
CCL11	closed w_a ΛCDM, m_ν	0.3	0.05	0.75	0.7	0.8	0.96	-0.9	0.1	3	{0.03, 0.02, 0}

Table 4. Cosmological models with massive neutrinos used in testing `CCL` against independently produced benchmarks
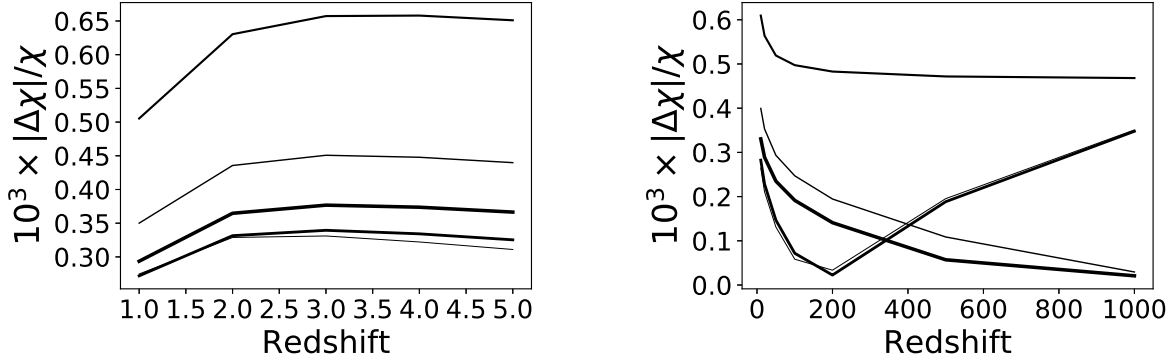
Figure 3. Accuracy achieved by `CCL` in the prediction of distances for models CCL7-11 with massive neutrinos, documented in Table 4. Different models correspond to different thickness curves. The left panel represent the accuracy checks at low redshift, while the right panel demonstrates accuracy up to high redshift. Note that we allow up to 10^{-3} fractional difference between benchmarks and `CCL` in this case, because benchmarks utilize a fitting function for the neutrino phase space integral which is itself not accurate to 10^{-4}.

trum, we obtained similar accuracy at $z = 0$ for the same wavenumbers. The cosmologies for which the tests were implemented are specified in Table 2.

The BCM implementation for the impact of baryons on the matter power spectrum, described in Section 2.3 is also analytical, and accurate to 10^{-12}.

4.2.2. *Validation of interpolation schemes*

Volunteer(s) in charge: Elisa Chisari, Christiane Lorenz

In its default configuration, `CCL` adopts the HaloFit (Takahashi et al. 2012) implementation by interpolating `CLASS` power spectra outputs to model the matter power spectrum. The computation of the power spectrum from `CLASS` can be significantly sped up by interpolating the matter power spectra in the range `K_MIN` $< k <$ `K_MAX_SPLINE` and extrapolating beyond it, as described in Section 3. In this section, we describe the loss of accuracy due to this method. The tests presented are performed in a flat ΛCDM cosmology with $\Omega_c = 0.25$, $\Omega_b = 0.05$, $A_s = 2.1 \times 10^{-9}$, $h = 0.7$ and $n_s = 0.96$.

The accuracy of this approximation is shown in Figure 4 for redshifts $z = 0$, $z = 3$ and $z = 20$. We compare the nonlinear matter power spectrum at these redshifts, computed with the previously described approximation, to the matter power spectrum obtained by setting the power spectrum splines to high-accuracy values. We find that for typical values of $\Delta \ln k = 10^{-2}$ and `K_MAX_SPLINE`$= 50$/Mpc, $\ln P$ has converged to an accuracy that surpasses the expected impact of baryonic effects on the matter power spectrum at $k > 10$/Mpc. (For an estimate of the impact of baryons on the total matter power spectrum, see Schneider & Teyssier 2015.)

With the implementation described above, the power spectrum splines are initialized up to `K_MAX_SPLINE`. This is also true for the linear matter power spectrum, which is used within `CCL` in particular to obtain σ_8 (see Eq. 42). We have tested how this procedure affects the convergence of the linear matter power spectrum. We compare the fiducial `CCL` output to the case where we set `K_MAX_SPLINE` $= 5 \times 10^3$/Mpc. The result is shown in Figure 4. For some applications that use the linear power spectrum, the user might need to increase the value of `K_MAX_SPLINE`. While `CCL` adopts certain fidu-
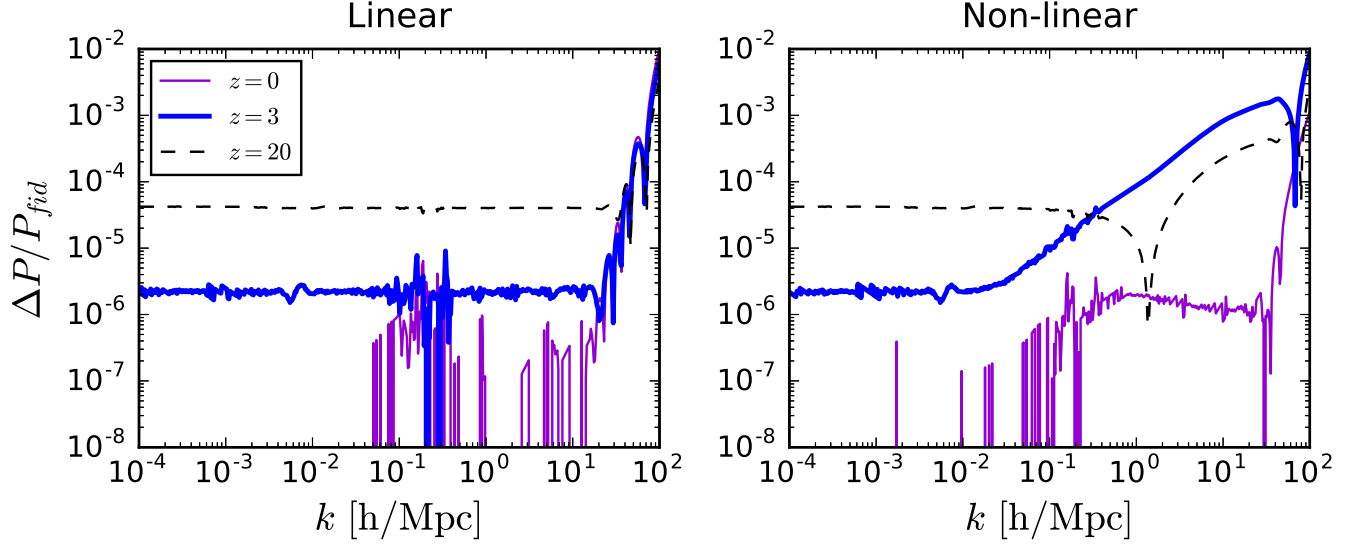
Figure 4. The relative error compared to power spectra produced with high values of the power spectrum splines, P_{fid}, produced by splining the matter power spectrum up to `K_MAX_SPLINE` and extrapolating beyond this value with a second order Taylor expansion the natural logarithm of the matter power spectrum. The left panel shows the relative errors for the linear matter power spectrum at $z = 0$, $z = 3$ and $z = 20$. The right panel shows the results for the non-linear matter power spectrum at the same redshifts. The standard `CCL` parameters adopted are those corresponding to the black dashed curve. For comparison, the impact of baryonic physics on the matter power spectrum is $\sim 10\%$ at $k = 1/\mathrm{Mpc}$ (Schneider & Teyssier 2015).

cial values of the number of scale factor and wavenumber values to use in the interpolation, we have tested that increasing the sampling does not change the results presented in Figures 4.

In addition to the above tests in ΛCDM cosmologies without massive neutrinos, we have checked the impact of using splines at low and high k in cosmologies CCL7, CCL8, and CCL9 with massive neutrinos, defined in Table 4. We compare the linear and nonlinear matter power spectrum as computed directly via `CLASS` to that computed using `CLASS` via `CCL` (i.e. using splines at high and low k). We find that for k between `K_MIN` and `K_MIN_SPLINE`, the two power spectra agree to better than 10^{-4} in all models. For k between `K_MAX_SPLINE` and `K_MAX`, agreement is better than 10^{-3}, which we deem sufficient given the significant uncertainties introduced at these small scales, e.g. baryonic effects. The fractional difference between the two power spectra is plotted in Figure 5. To do: Are we okay with this? -DL

4.2.3. *Generalized validation of the power spectrum over* ΛCDM *parameter space*

Volunteer(s) in charge: Phil Bull Suggested content: 'Fair' sampling of parameter space with Latin Hypercubes. Summary statistics used, and binning of power spectrum in k and z. Precision settings used for CLASS. Estimates of run-time. Results. Range of validity.
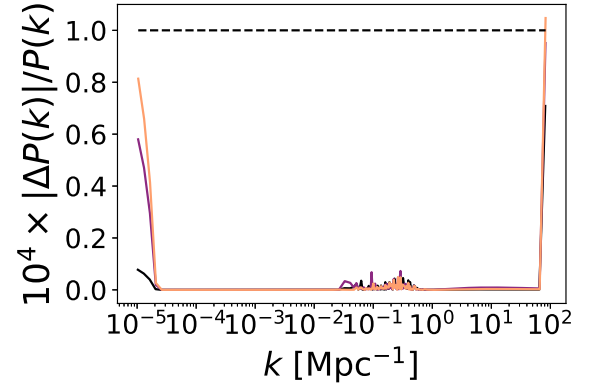
Figure 5. Fractional difference between the nonlinear matter power spectrum as computed directly via `CLASS` with that computed using `CLASS` via `CCL` in cosmologies CCL7, CCL8, and CCL9 with massive neutrinos.

To do: Have the undergraduate students who did most of this work been included as authors on the paper? - DL

While concentrating on individual points in cosmological parameter space allows us to perform detailed validation tests, as above, it is important for `CCL` to also be validated across a wide range of cosmological parameter values, e.g. to ensure validity for MCMC analyses. In this section, we present a set of validation tests for the `CCL` linear and non-linear matter power spectrum functions that spans a broad range of ΛCDM parameters.

Covering a full range of all 5 ΛCDM parameters on a regular grid would be prohibitively expensive, so an alternative method for fairly (but more sparsely) sampling the parameter space is needed. We use Latin Hypercube Sampling to determine a tractably-sized set of sample points. This splits the parameter space into a regular grid with a given number of cells per dimension. The sample points are then chosen by going through each dimension in turn and choosing a cell at random *without replacement*, so that a given cell of a given dimension is only ever chosen once. This is repeated until all cells in all dimensions contain a single sample. This has the effect of covering the space uniformly but sparsely. The exact location of the sample within each cell can be chosen from a uniform distribution within that cell, but for simplicity we put each sample at the cell centre. The ranges used for each parameter are shown in Table 5.

Parameter	Range
h	$[0.5, 0.9]$
Ω_c	$[0.1, 0.4]$
Ω_b	$[0.018, 0.052]$
A_s	$[1.5 \times 10^{-9}, 2.5 \times 10^{-9}]$
n_s	$[0.93, 0.99]$

Table 5. Ranges of ΛCDM parameters used for the generalised `CCL` validation tests of the matter power spectrum.

For each set of parameters, we then calculate the linear and non-linear power spectra using `CCL` for a range of redshifts ($z \in \{0, 0.5, 1, 1.5, 2, 2.5\}$) and wavenumbers ($k \in [10^{-4}, 10^0]$ Mpc^{-1}). A corresponding set of reference power spectra is then produced using `CLASS`, which we run with settings chosen to produce high-precision results, taken from the `pk_ref.pre` precision file that is bundled with `CLASS`.

To quantify the level of agreement between the `CCL` and reference power spectra, we use the following summary statistic that can be summed over a chosen set of bins in redshift and wavenumber:

$$\Delta = \sum_{ij} \Theta \left(\log_{10} \left| \frac{P_{\text{CCL}}(k_i, z_j) - P_{\text{ref}}(k_i, z_j)}{P_{\text{ref}}(k_i, z_j)\Delta_{\text{thres}}} \right| \right). \quad (75)$$

Here, Δ_{thres} is a target threshold for the fractional deviation between the power spectra, and we have defined $\Theta(x) \equiv x \ \ (x \geq 0)$ and 0 otherwise. Bins where the `CCL` power spectrum deviates from the reference power spectrum by a fraction less than Δ_{thres} do not contribute to the statistic, so the aim is to have $\Delta = 0$ (i.e. no deviation beyond the threshold in any bin). If deviations are found, however, they are weighted logarithmically –

one large deviation of several orders of magnitude affects the statistic as much as a few smaller deviations of order $\sim \Delta_{\text{thres}}$. To do: This section still needs discussion and conclusions, right? -DL

4.2.4. *Validation of the Cosmic Emulator implementation*

Volunteer(s) in charge: Elisa Chisari To do: I think this section should go before the one on generalized validation of the power spectrum over LCDM space, because that one refers to 'the sections above' as being at specific cosmologies, which is the case here. - DLTo do: The only caveat is that the generalized validation scheme doesnt account for the emulator - EC. Lawrence et al. (2017) quantified the accuracy of the matter power spectrum from their emulation scheme by comparing their predictions to the resulting power spectra from the numerical simulations used for the calibration of their scheme. We repeated this procedure making the emulator predictions via `CCL` for a subset of emulator cosmologies.

Our results, presented in the form of absolute fractional accuracy of the power spectra, are shown in Figure 6. For cosmologies without neutrinos, we required the matter power spectrum at $z = 0$ to be within 1% of the smoothed simulated power spectrum from Lawrence et al. (2017) (see their Figure 6). Similarly, we required 3% accuracy for cosmologies with neutrinos (their Figure 5). The cosmologies that were tested are the ones listed in Table 3, which are described in detail in Lawrence et al. (2017).

4.3. *Halo bias and halo mass function*

Independent codes were utilized to test the accuracy of halo mass function predictions. These predictions are computed from power spectra obtained using the BBKS approximation. For the halo mass function, we compare the value of σ, $\log(\sigma^{-1})$, and the value of the halo mass function in the form used in Tinker et al. (2008),

$$\log[(M^2/\bar{\rho}_m)dn/dM]. \quad (76)$$

We note that while we maintain the 10^{-4} for our evaluations of σ, the accuracy degrades to a value of 5×10^{-3} for the halo mass function evaluation, primarily at the high halo mass and high redshift domains. We find that this increased error is acceptable, as the level of precision is significantly better than the accuracy of current halo mass function models. This is demonstrated in Figure 7, where this calculation has been run for a single cosmology using the Tinker 2010 halo mass function. While there is a degradation in accuracy due to our current spline treatment of the log inverse of $\sigma(M)$, we note that it does not significantly degrade our halo mass function determination. While improvement on

Figure 6. Absolute fractional accuracy in the matter power spectra obtained by calling the cosmic emulator from `CCL` and the smoothed simulated spectra from (Lawrence et al. 2017). The left panel shows the results for cosmologies without neutrinos; the right panel, results for cosmologies with neutrinos.

this remains a task for the future, the halo mass function varies between fitting functions significantly more than this remaining error. As of this time, we currently do not have independent benchmarks for the halo bias function, though it should be noted that this calculation does not involve any additional functions beyond $\sigma(M)$ and should hold to the 10^{-4} tolerance level.

4.4. Two-point statistics

We used the BBKS linear matter power spectrum to compare two-point statistics for two redshift bins, resulting in three tomography combinations, $(1-1),(1-2),(2-2)$. We computed the following quantities:

- Number counts angular power spectra: density term only (no magnification, RSD, etc.) with non-evolving linear bias $b(z) = 1$, in the range $10 < \ell < 10000$, using 5 bins per decade,

- Lensing convergence angular power spectra: leading order convergence term only (no magnification or intrinsic alignments), in the same range and with the same resolution as the case above,

- Number counts angular correlation functions in the range $0.01\,\deg < \theta < 5\,\deg$, using 5 bins per decade, and

- Lensing shear angular correlation functions (ξ_+,ξ_-), similarly to above.

We adopted the following analytic redshift distributions: a Gaussian with $\sigma = 0.15$, centered at $z_1 = 1$; and another Gaussian with the same dispersion but centered at $z_2 = 1.5$. We repeated the exercise for two redshift distribution histograms shown in Figure 8. Besides these two-point functions, we also validated the computation of the CMB lensing power spectrum, using the same ℓ binning described above.

For C_ℓ computations, we achieved a relative difference between `CCL` and the benchmarks of $< 10^{-3}$ (3×10^{-3} for CMB lensing). This applied both to analytic redshift distributions and histograms, for auto- and cross-correlations between bins for both galaxy clustering and weak lensing, as shown in Figure 9. The CMB lensing result is shown in Figure 10.

To obtain realistic targets for the convergence of projected correlation function computations for LSST analyses, we calculated the expected statistical uncertainty of the clustering and lensing correlation functions of the LSST gold sample To do: Add reference assuming an effective source galaxy density of $n_{\rm eff} = 26\,{\rm gal/sq\,arcmin}$ for galaxy shape distortions, and galaxy density of $n_{\rm gold} = 45\,{\rm gal/sq\,arcmin}$ for number counts. Specifically, we calculated the Gaussian covariance of angular correlation functions following the formalism of Joachimi et al. (2008), and note that leaving out the non-Gaussian covariance terms makes our accuracy criterion more conservative. We split the galaxy samples into 10 tomography bins, defined to contain equal numbers of galaxies. The accuracy test then proceeded as follows. We compared the difference between `CCL` calculated lensing and clustering correlations and the benchmarks, for the analytic redshift distributions and for auto-correlations of redshift bins only. To pass the benchmark test, we required that this difference be smaller than half of the value of the error bar derived from the covariance for each correlation function computed. Specifically, we took the value of the covariance in the bins centered at $z = 1$ and $z = 1.5$ to compare to the benchmarks.

The results of this validation procedure for the projected correlation function are shown in Figure 11. Our results suggest that the convergence between `CCL` pre-
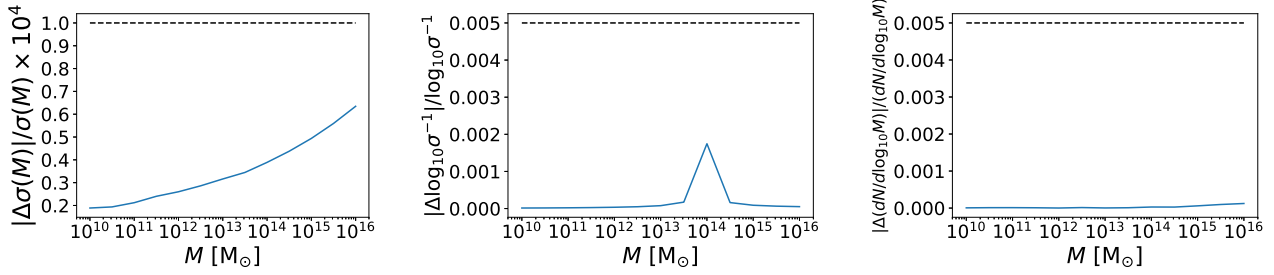
Figure 7. Three different numerical tests of the halo mass function calculation. In each line, the blue line is the fractional error in the function, while the black dashed line represents our error tolerance. The first panel demonstrates the robust calculation of $\sigma(M)$. The second panel demonstrates a numerical quirk in our spline treatment that is currently not addressed, but does reduce the numerical accuracy in returning the log inverse of $\sigma(M)$. We note that this does not significantly impact the error in the halo mass function in the final panel.
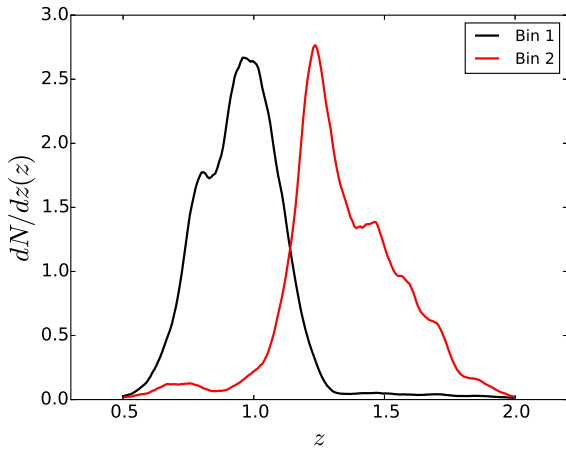
Figure 8. Binned redshift distributions used for code comparison project.

dictions and benchmarks is below the expected statitical uncertainty.

The 3-dimensional spatial correlation function $\xi(r)$ was validated by comparing with an independent, precise numerical transform. We calculated $\xi(r)$ by transforming the CCL non-linear HaloFit power spectrum using this independent code for the five cosmologies listed in Table 3 at redshifts $z = 0, 1, 2, 3, 4, 5$. We then compared with the $\xi(r)$ from CCL with a sampling of $P(k)$ equal to N_K_3DCOR bins per decade. The default value of N_K_3DCOR $= 100,000$ results in a relative agreement at the level of $\Delta\xi(r)/\xi(r) < 2.5 \times 10^{-3}$ for $0.1 < r < 250$ Mpc and $z = 0$. The agreement was better for higher redshifts. We also compared the absolute value of $r^2\xi(r)$ and find a maximum difference of $\Delta(r^2\xi(r)) < 3.0 \times 10^{-2}$ for the range $r = 0.1 - 250$ Mpc. This corresponds to approximately 0.08% of the Baryon Acoustic Oscillation peak value of $r^2\xi(r)$. At the peak, the difference is only 9.0×10^{-3}, or 0.024% of the peak height. The results are shown in Fig. 12

To further validate the $P(k) \rightarrow \xi(r)$ transform we performed a test using an analytical function $\xi(r) = (r/r_0)^a$, whose inverse transform $P(k)$ has a known analytic form. We used $r_0 = 5h^{-1}$ Mpc^{-1} and $a = -1.67$, which approximates the actual three-dimensional correlation function. We then compared the CCL calculation of $\xi(r)$ to the known analytic result. The relative difference $\Delta\xi(r)/\xi(r)$ was found to be less than 0.4% in the range $1 < r < 200$ Mpc rising to about 5% at $r = 1000$ Mpc (see Fig. 13). For $r = 0.1 - 0.8$ Mpc the relative difference is $\approx 8\%$. The accuracy at low and high distances can be improved by increasing the range over which the power spectrum splines are evaluated.

4.4.1. Angpow

CCL performs non-Limber computations of angular power spectra through the Angpow library as detailed in Section 3.3.2. The Angpow software was tested against CLASS and the native CCL computation and can perform the same computations approximately an order of magnitude faster ($\mathcal{O}(1s)$). Its precision and speed parameters were optimised so that the relative numerical error compared with a high precision computation is two orders of magnitude below the relative cosmic variance $\sqrt{2/(2\ell + 1)}$, from $\ell = 2$ to $\ell = 1000$. We demonstrate this in Figure 14, where we plot the angular clustering power spectrum for a sample of galaxies with $\langle z \rangle = 1$ and a Gaussian redshift distribution that extends between $|z - \langle z \rangle| < 5\sigma_z$, where $\sigma_z = 0.02$, for a CCL6 cosmology. The non-Limber prediction deviates from the Limber case at low l as expected. The right panel shows the fractional difference between the non-Limber curves, demonstrating the accuracy of the Angpow prediction for our choice of precision and speed prameters. Also the native non-Limber computation and Angpow where tested to recover the Limber approximated curve at high l for a wide Gaussian window ($\sigma_z = 0.1$). The relative errors with respect to the Limber result at high

Figure 9. Tests of the angular power spectrum accuracy. Benchmark comparisons for number counts (solid) and weak lensing (dashed) power spectra are shown for analytic and histogram-based redshift distributions in the left and right panels respectively..
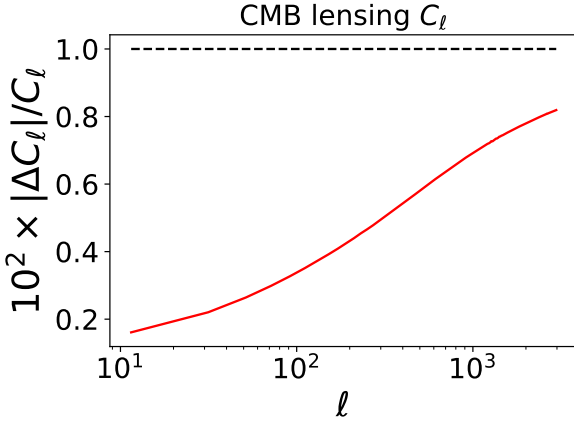

Figure 10. Same as Fig. 9 for the CMB lensing power spectrum **probably explain here why we achieve a worse accuracy here**.

l are below two orders of margnitudes with respect to cosmic variance.

5. USAGE

Volunteer(s) in charge: Renee,Elisa **Section ready for revision**

CCL is a public tool developed by the members of the Dark Energy Science Collaboration of LSST and can be downloaded from the collaboration's github repository at the URL provided in the abstract. Installation instructions are provided in a README file available in that same repository. Instructions on how to generate a Docker[11] image are provided for portability to different architectures. CCL dependencies include the GNU Sci-

entific Library[12] and FFTW3[13]. A suite of tests can be run to ensure installation was successful and all features perform nomrmally. Accuracy checks are performed in C, while a suite of unit tests is available in python.

CCL is documented using Doxygen[14]. For convenience, the repository includes multiple example files in C and several Jupyter notebooks.

CCL is released under terms consistent with BSD 3-Clause licensing MI: Maybe a reference here.

6. OUTLOOK

Volunteer(s) in charge: David Alonso, Elisabeth Krause **Section ready for revision**

Science software development to facilitate the cosmological inference from LSST data is one of the critical tasks of the Dark Energy Science Collaboration (DESC). Recent cosmological analyses of the Dark Energy Survey (DES) relied on CosmoSIS (Zuntz et al. 2014) and CosmoLike (Krause et al. 2017), the Kilo-Degree Survey (KiDS) uses CosmoMC (Lewis & Bridle 2002); all three frameworks employ CLASS, CAMB (Challinor & Lewis 2005), or the cosmic emulator to compute the density power spectra. Compared to the analyses of DES, KiDS and the Hyper-Suprime Cam Survey (HSC), future data sets (e.g. LSST, *Euclid* and *WFIRST*) have substantially higher demands on analysis frameworks. Analyses are becoming more complex in terms of cosmological physics that is included in the analyses (neutrinos, modified gravity, and dark matter models) and in terms of modeling astrophysical and observational systematics at the required precision.
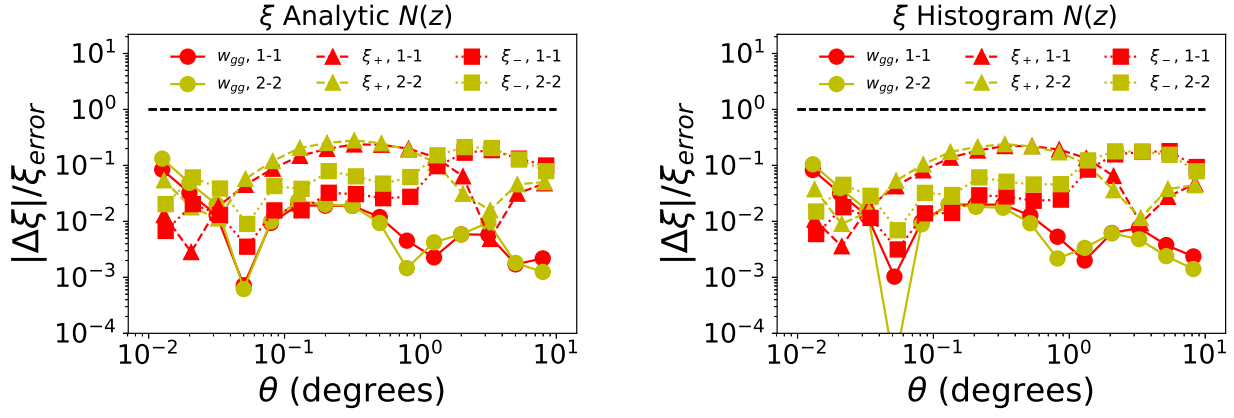
Figure 11. Comparison between the predicted projected correlation functions and the expected uncertainties for LSST. The left panel shows predictions for the analytic redshift distrobutions, while the right panel shows the case of the redshift histograms. The different markers and colors indicate clustering (w_{gg}, filled circles) or lensing ($\xi_\pm$, filled triangles and squares) auto-correlations of the 1-1 or 2-2 redshift bin combinations.
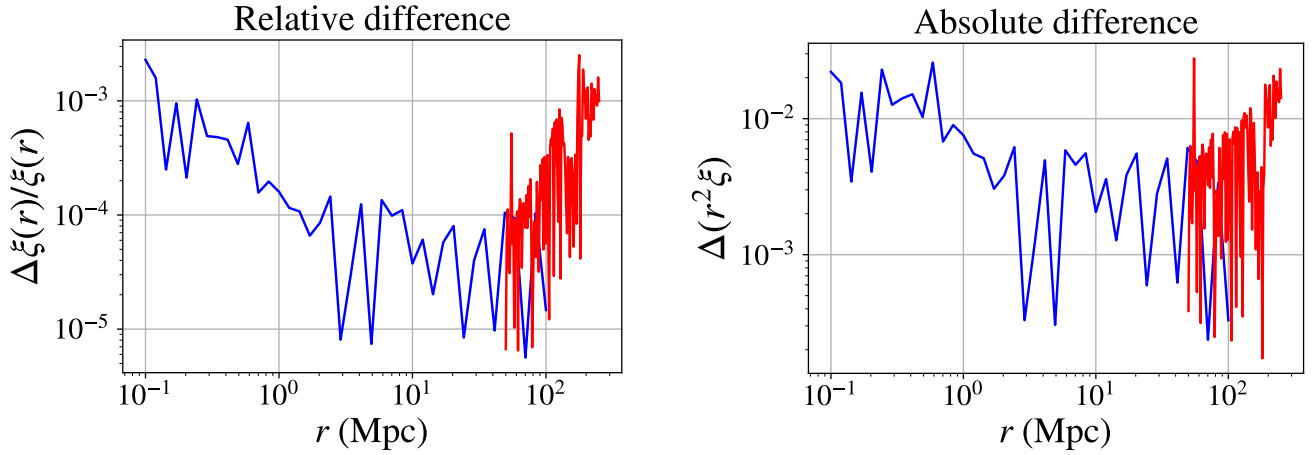

Figure 12. Comparison of the CCL calculation of the three-dimensional spatial correlation function $\xi(r)$ with a precise, numerical transform of the `CCL` non-linear Halofit power spectrum. The left panel shows the relative error $\Delta\xi(r)/\xi(r)$. The right panel shows the absolute error in $r^2\xi(r)$. Both panels are for the w_a LCDM model of Table **??** at redshift zero. MI: Which models: there seems to be a typo.

It is the primary goal of the `CCL` to become the backbone of all cosmological analyses carried out by the Dark Energy Science Collaboration of the LSST. This unified approach of a validated `CCL` will ensure that DESC results that are both consistent (in that they will all be based on the same theory framework) and accurate (in that this framework has undergone a rigorous numerical validation).

The implementation of `CCL` in realistic analysis pipelines has already begun: all likelihood module prototypes under development use it as its backbone, and the first of these, cosmological analysis of angular galaxy clustering cross-correlations, will serve as a model for the design of the joint-probes likelihood of the DESC. This work has allowed us to validate the performance of `CCL` in a realistic analysis scenario, verifying its ac-

curacy and efficiency in the context of computationally demanding MCMC runs.

Beyond its usefulness in the DESC, the flexible design of `CCL` makes it a useful tool for the analysis of other cosmological datasets, as well as for the cross-correlation of different experiments. To this end, and to allow a generic and flexible analysis of the LSST data, further functionality will be added to `CCL`. Plans are in place to extend the range of standard and non-standard cosmological models covered by the code. Work is already underway to add a comprehensive implementation of the halo-model calculation of two-point functions (Peacock & Smith 2000) with sufficient flexibility to include generic parametrizations of observable halo profiles and mass-observable relations. The current simplified treatment of the galaxy-matter connection for galaxy clus-
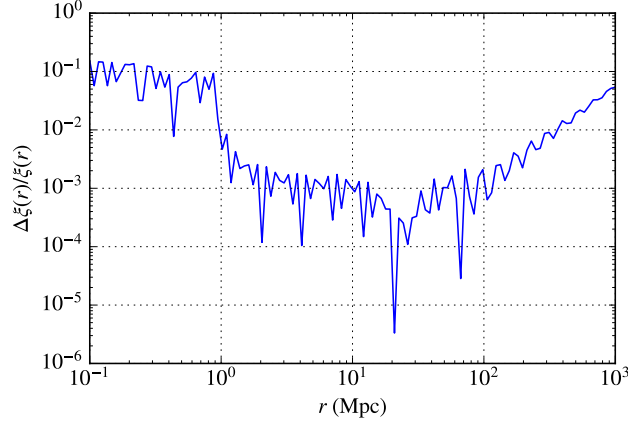
Figure 13. The relative error in the three-dimensional spatial correlation function computed using the CCL algorithm compared to an analytic function $\xi(r) = (r/r_0)^a$ whose inverse transform $P(k)$ is known analytically. In this validation test, the known $P(k)$ was transformed with the CCL algorithm and compared to the known analytic result for $\xi(r)$.
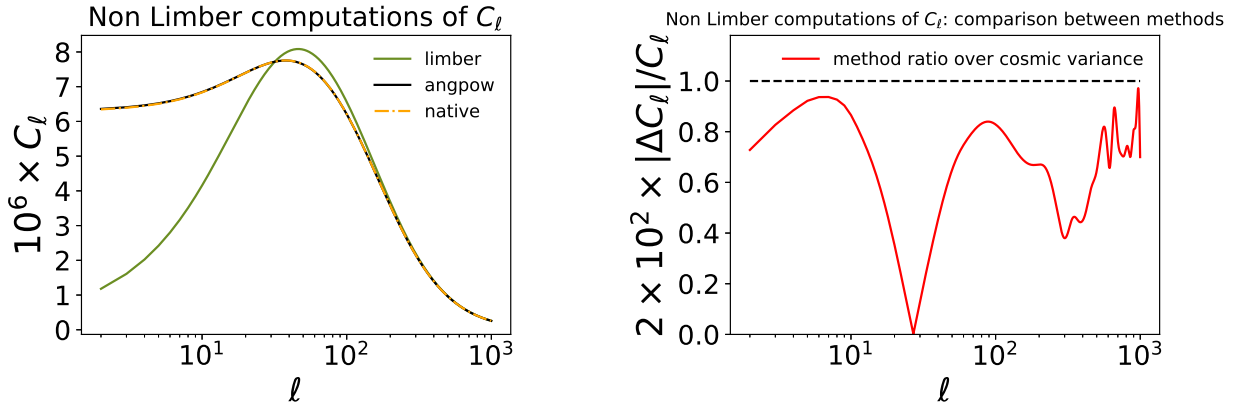

Figure 14. Different predictions for the clustering angular power spectrum of a sample of galaxies with a Gaussian redshift distribution centered on $\langle z \rangle = 1$. The left panel shows the C_l predictions from the Limber case (green), the non-Limber case native to CCL (yellow dot-dashed) and Angpow (black). The right panel shows the fractional difference in the predicted clustering angular power spectrum between Angpow and the native CCL non-Limber computation. The relative numerical error compared with a high precision computation is two orders of magnitude below the relative cosmic variance: $\sqrt{2/(2\ell + 1)}$. To do: Fix margins of right panel

tering and intrinsic alignments will be improved by implementing generic perturbation-theory approaches to structure formation (McDonald & Roy 2009; McEwen et al. 2016). A more complete implementation of all relevant cross-correlations between large-scale structure observables and other cosmological probes (e.g. CMB integrated Sachs-Wolfe effect, Sachs & Wolfe 1967, and other secondary anisotropies) will also soon be included. MI: Did you mean to have the citation to Sachs-Wolfe in that format?

In general, although this document presents the functionality and performance of CCL shortly after its release, we expect the library to be a continuously evolving piece of software. This will allow CCL to satisfy the analysis needs of future large datasets, as well as more accurate and sophisticated models for a broad range of cosmological and astrophysical observables.

Author contributions are listed below.

Husni Almoubayyed: Reviewed code/contributed to issues.

David Alonso: Co-led project; developed structure for angular power spectra; implemented autotools; integrated into LSS pipeline; contributed to: background, power spectrum, mass function, documentation and benchmarks; reviewed code

Jonathan Blazek: Planning capabilities and structure; documentation and testing.

Philip Bull: Implemented the Python wrapper and wrote documentation for it; general bug fixes, maintenance, and code review; enhanced the installer and error handling system.

Jean-Éric Campagne: Angpow main builder.

N. Elisa Chisari: Co-led project, coordinated hack projects & communication, contributed to: correlation function & power spectrum implementation, documentation, and comparisons with benchmarks.

Alex Drlica-Wagner: Helped with document preparation.

Zilong Du: Implemented the 3d correlation function.

Tim Eifler: Reviewed/tested code.

John Ellison: Implemented the 3d correlation function; documentation of 3d correlation function.

Renée Hlozek: Contributed initial code for error handling structures, reviewed other code edits.

Mustapha Ishak: Contributed to planning of code capabilities and structure; reviewed code; identified and fixed bugs; wrote text for this note.

Shahab Joudaki: Created physical density function and documentation.

Matthew Kirby: Performed comparison of physical constants.

David Kirkby: Writing, testing and reviewing code. Asking questions.

Elisabeth Krause: Initiated and co-led project; developed CLASS interface and error handling; contributed to other code; reviewed pull requests.

C. Danielle Leonard: Wrote and tested code for LSST specifications, user-defined photo-z interface, and support of neutrinos; reviewed other code; wrote text for this note.

Christiane S. Lorenz: Contributed to accurate high-redshift cosmological background quantities and benchmarked background splines.

Phil Marshall: Helped with document preparation.

Thomas McClintock: Wrote Python and doxygen documentation.

Sean McLaughlin: Wrote doxygen documentation and fixed bugs/added functionality to distances.

Alexander Mead: Wrote halo-model code and documentation

Jérémy Neveu: Contributed to Angpow, built the interface with CCL and the comparisons with benchmarks.

Stéphane Plaszczynski: Contributed to Angpow.

Javier Sanchez: Modified setup.py to allow pip installation and uninstall.

Sukhdeep Singh: Contributed to the correlation functions code.

Anže Slosar: Wrote and reviewed code.

Antonio Villarreal: Contributed to initial benchmarking, halo mass function code, and general code and issues review.

Michal Vrastil: Wrote documentation and example code, reviewed code.

Joe Zuntz: Wrote initial infrastructure, C testing setup, and reviewed code.

REFERENCES

Alonso, D., Bull, P., Ferreira, P. G., Maartens, R., & Santos, M. G. 2015, ApJ, 814, 145

Alonso, D., & Ferreira, P. G. 2015, PhRvD, 92, 063525

Angulo, R. E., Springel, V., White, S. D. M., et al. 2012, MNRAS, 426, 2046

Astropy Collaboration, Robitaille, T. P., Tollerud, E. J., et al. 2013, A&A, 558, A33

Bardeen, J. M., Bond, J. R., Kaiser, N., & Szalay, A. S. 1986, ApJ, 304, 15

Bartelmann, M., & Schneider, P. 2001, PhR, 340, 291

Beringer, J., et al. 2012, Phys. Rev., D86, 010001

Blas, D., Lesgourgues, J., & Tram, T. 2011, CLASS: Cosmic Linear Anisotropy Solving System, Astrophysics Source Code Library, ascl:1106.020

Blazek, J., MacCrann, N., Troxel, M. A., & Fang, X. 2017, ArXiv e-prints, arXiv:1708.09247

Bonvin, C., & Durrer, R. 2011, PhRvD, 84, 063505

Bullock, J. S., Kolatt, T. S., Sigad, Y., et al. 2001, MNRAS, 321, 559

Campagne, J.-E., Neveu, J., & Plaszczynski, S. 2017a, ArXiv e-prints, arXiv:1701.03592

Campagne, J.-E., Plaszczynski, S., & Neveu, J. 2017b, ApJ, 845, 28

Carroll, S. M. 2001, Living Reviews in Relativity, 4, 1

Castorina, E., Carbone, C., Bel, J., Sefusatti, E., & Dolag, K. 2015, JCAP, 7, 043

Challinor, A., & Lewis, A. 2005, PhRvD, 71, 103010

—. 2011, PhRvD, 84, 043516

Chevallier, M., & Polarski, D. 2001, International Journal of Modern Physics D, 10, 213

Chon, G., Challinor, A., Prunet, S., Hivon, E., & Szapudi, I. 2004, MNRAS, 350, 914

Cooray, A., & Sheth, R. 2002, Physics Reports, 372, 1

Copeland, E. J., Sami, M., & Tsujikawa, S. 2006, International Journal of Modern Physics D, 15, 1753

DES Collaboration, Abbott, T. M. C., Abdalla, F. B., et al. 2017, ArXiv e-prints, arXiv:1708.01530

Dodelson, S. 2004, Modern Cosmology, Vol. 57, 60–61, doi:10.1063/1.1784308

Durrer, R. 2008, The Cosmic Microwave Background (Cambridge University Press)

Eifler, T., Krause, E., Dodelson, S., et al. 2015, MNRAS, 454, 2451

Eisenstein, D. J., & Hu, W. 1998, ApJ, 496, 605

Frigo, M., & Johnson, S. G. 2012, FFTW: Fastest Fourier Transform in the West, Astrophysics Source Code Library, ascl:1201.015

Ghosh, B., Durrer, R., & Sellentin, E. 2018, ArXiv e-prints, arXiv:1801.02518

Giocoli, C., Bartelmann, M., Sheth, R. K., & Cacciato, M. 2010, MNRAS, 408, 300

Green, J., Schechter, P., Baltay, C., et al. 2011, ArXiv e-prints, arXiv:1108.1374

Hamilton, A. J. S. 2000, MNRAS, 312, 257

Heitmann, K., Bingham, D., Lawrence, E., et al. 2016, ApJ, 820, 108

Hellwing, W. A., Schaller, M., Frenk, C. S., et al. 2016, MNRAS, 461, L11

Hildebrandt, H., Viola, M., Heymans, C., et al. 2017, MNRAS, 465, 1454

Hirata, C. M., Mandelbaum, R., Ishak, M., et al. 2007, MNRAS, 381, 1197

Hirata, C. M., & Seljak, U. 2004, PhRvD, 70, 063526

Ishak, M. 2007, Foundations of Physics, 37, 1470

Joachimi, B., & Bridle, S. L. 2010, A&A, 523, A1

Joachimi, B., Schneider, P., & Eifler, T. 2008, A&A, 477, 43

Joudaki, S., Blake, C., Johnson, A., et al. 2018, MNRAS, 474, 4894

Kamionkowski, M., & Spergel, D. N. 1994, ApJ, 432, 7

Kitching, T. D., & Heavens, A. F. 2017, PhRvD, 95, 063522

Krause, E., Eifler, T., & Blazek, J. 2016, MNRAS, 456, 207

Krause, E., Eifler, T. F., Zuntz, J., et al. 2017, ArXiv e-prints, arXiv:1706.09359

Lattanzi, M., & Gerbino, M. 2017, ArXiv e-prints, arXiv:1712.07109

Laureijs, R., Amiaux, J., Arduini, S., et al. 2011, ArXiv e-prints, arXiv:1110.3193

Lawrence, E., Heitmann, K., Kwan, J., et al. 2017, ApJ, 847, 50

Lesgourgues, J., & Pastor, S. 2012, ArXiv e-prints, arXiv:1212.6154

Lewis, A., & Bridle, S. 2002, PhRvD, 66, 103511

Linder, E. V. 2003, Physical Review Letters, 90, 091301

LSST Dark Energy Science Collaboration. 2012, ArXiv e-prints, arXiv:1211.0310

McDonald, P., & Roy, A. 2009, JCAP, 8, 020

McEwen, J. E., Fang, X., Hirata, C. M., & Blazek, J. A. 2016, JCAP, 9, 015

Mo, H. J., & White, S. D. M. 1996, MNRAS, 282, 347

Mohammed, I., & Gnedin, N. Y. 2017, ArXiv e-prints, arXiv:1707.02332

Mohammed, I., & Seljak, U. 2014, MNRAS, 445, 3382

Navarro, J. F., Frenk, C. S., & White, S. D. M. 1997, ApJ, 490, 493

Ng, K.-W., & Liu, G.-C. 1999, International Journal of Modern Physics D, 8, 61

Padmanabhan, T. 2003, PhR, 380, 235

Peacock, J. A. 1999, Cosmological Physics, 704

Peacock, J. A., & Smith, R. E. 2000, MNRAS, 318, 1144

Peebles, P. J., & Ratra, B. 2003, Reviews of Modern Physics, 75, 559

Sachs, R. K., & Wolfe, A. M. 1967, ApJ, 147, 73

Schneider, A., & Teyssier, R. 2015, JCAP, 12, 049

Seljak, U. 2000, MNRAS, 318, 203

Semboloni, E., Hoekstra, H., & Schaye, J. 2013, MNRAS, 434, 148

Semboloni, E., Hoekstra, H., Schaye, J., van Daalen, M. P., & McCarthy, I. G. 2011, MNRAS, 417, 2020

Sheth, R. K., Mo, H. J., & Tormen, G. 2001, MNRAS, 323, 1

Smith, R. E., & Markovic, K. 2011, PhRvD, 84, 063507

Smith, R. E., Scoccimarro, R., & Sheth, R. K. 2007, PhRvD, 75, 063512

Springel, V., Pakmor, R., Pillepich, A., et al. 2017, ArXiv e-prints, arXiv:1707.03397

Takahashi, R., Sato, M., Nishimichi, T., Taruya, A., & Oguri, M. 2012, ApJ, 761, 152

Talman, J. 2009, Computer Physics Communications, 180, 332

Tinker, J., Kravtsov, A. V., Klypin, A., et al. 2008, ApJ, 688, 709

Tinker, J. L., Robertson, B. E., Kravtsov, A. V., et al. 2010, ApJ, 724, 878

Troxel, M. A., & Ishak, M. 2015, PhR, 558, 1

Upadhye, A., Biswas, R., Pope, A., et al. 2014, PhRvD, 89, 103515

van Daalen, M. P., Schaye, J., Booth, C. M., & Dalla Vecchia, C. 2011, MNRAS, 415, 3649

van Uitert, E., Joachimi, B., Joudaki, S., et al. 2018, MNRAS, arXiv:1706.05004

Vogelsberger, M., Genel, S., Springel, V., et al. 2014, Nature, 509, 177

Watson, W. A., Iliev, I. T., D'Aloisio, A., et al. 2013, MNRAS, 433, 1230

Weinberg, D. H., Mortonson, M. J., Eisenstein, D. J., et al. 2013, PhR, 530, 87

Yoo, J. 2010, PhRvD, 82, 083508

Yoo, J., Fitzpatrick, A. L., & Zaldarriaga, M. 2009, PhRvD, 80, 083514

Zumalacárregui, M., Bellini, E., Sawicki, I., Lesgourgues, J., & Ferreira, P. G. 2017, JCAP, 8, 019

Zuntz, J., Paterno, M., Jennings, E., et al. 2014, CosmoSIS: Cosmological parameter estimation, Astrophysics Source Code Library, ascl:1409.012